Chem Soc Rev

Strategies to create Hierarchical Self-Assembled Structures via Cooperative Non-covalent Interactions

Journal:	*Chemical Society Reviews*
Manuscript ID:	CS-REV-12-2014-000497.R1
Article Type:	Review Article
Date Submitted by the Author:	10-Feb-2015
Complete List of Authors:	Rest, Christina; Universität Würzburg, Institut für Organische Chemie Kandanelli, Ramesh; Universität Würzburg, Institut für Organische Chemie Fernandez, Gustavo; Universität Würzburg, Institut für Organische Chemie

Journal Name

RSCPublishing

ARTICLE

Cite this: DOI: 10.1039/x0xx00000x

Strategies to Create Hierarchical Self-Assembled Structures *via* Cooperative Non-Covalent Interactions

Christina Rest, Ramesh Kandanelli, Gustavo Fernández*

Received ooth January 2012,
Accepted ooth January 2012

DOI: 10.1039/x0xx00000x

www.rsc.org/

Cooperative phenomena are common processes involved in the hierarchical self-assembly of multiple systems in nature, such as the tobacco mosaic virus and cell cytoskeleton. Motivated by the high degree of order exhibited by these systems, a great deal of effort has been devoted in the past two decades to design hierarchical supramolecular polymers by combining different classes of cooperative interactions. In this review, we have classified the field of supramolecular polymers depending on the cooperative non-covalent forces driving their formation, with particular emphasis on recent examples from literature. We believe that this overview would help scientists in the field to design novel self-assembled systems with improved complexity and functionalities.

1. Introduction

The description of cooperative mechanism has evolved a long way from a biological perspective (e.g. enzyme activity or molecular sensing) to the creation of supramolecular structures. For this reason, a single point definition that covers all aspects of cooperativity would certainly admit some debate. Ercolani mentioned more than a decade ago that "cooperativity takes place when the binding of one ligand influences the binding strength of a macromolecule toward a subsequent ligand (or ligands)".[1] On the other hand, the concept was extended in the words of Anderson and Hunter as: "Cooperativity arises from the interplay of two or more interactions, so that the system as a whole behaves differently from expectations based on the properties of the individual interactions acting in isolation".[2] This vital concept of cooperativity is widespread in Nature.[3] One of the most representative and widely studied examples of cooperative phenomena in natural systems is the binding of O_2 to Fe in hemoglobin, where the binding affinity of hemoglobin towards oxygen increases with binding to every oxygen molecule.[4] Various other archetypal systems in nature such as the tobacco mosaic virus,[5-7] and biopolymeric walls of the cytoskeleton[8,9] self-assemble into highly-organized shape-persistent anisotropic nanostructures. In fact and as recently pointed out by Aida, Meijer and Stupp,[10] supramolecular polymeric structures with a high degree of order and multiple levels of hierarchy are the result of cooperative effects. An additional illustrative example in this regard that is ubiquitous in Nature is the self-assembly of *flagellin* molecules. Comprehensive investigations of the types and functional aspects of bacterial flagella[11,12] contrast with the considerably little attention devoted to their hierarchical self-assembly aspects. The basic structure of flagellum comprises three important subunits: a lengthy filament that is helical in nature, a hook and a stiff basal aspect that is incorporated into the cell membrane.[13,14] All subunits are in turn an assembly of a large number (thousands) of protein molecules called flagellins. The helical filaments are responsible for the locomotive function of the bacteria. A rough illustration of the flagellum structure of Gram negative bacterium is depicted in Fig. 1.

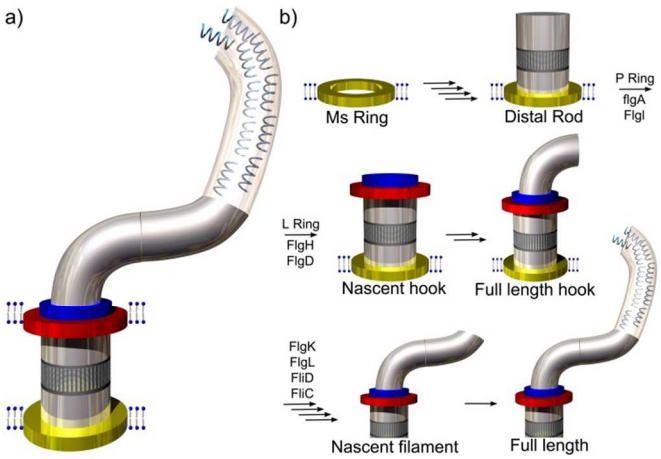

Fig. 1 a) General structure of the flagellum of a Gram-negative bacterium that depicts the key structural components in the form of MS ring, a distal rod, hook and a long filament. (b) A representation of systematic path of self-assembly starting after the formation of the MS ring to a fully formed flagellin filament that is helical in nature.

The self-assembly of flagellins starts from the cytoplasmic membrane. At each step, the self-assembly takes place through a simple condensation between the C- and N- terminals of the incoming protein and already attached protein, respectively. A clear illustration from Fig. 1 indicates that the initial step of the self-assembly is the formation of a MS-ring which is a set of five ring proteins that act as rotary motor. In subsequent steps, MS-ring development of the rod structure takes place by assembly of five rod proteins. Once the rod structure is formed,

initiation of hook formation takes place over P (periplasmic protein) and L (lipoprotein) rings. The last hierarchy level is the formation of the filament. This is facilitated by hook proteins, which make a junction in two stages so that a long filament building gets initiated that is completed with assembly of several numbers of proteins (about 20000).

In vitro analysis to monitor the self-assembly of flagellins confirmed that the process is thermodynamically favourable.[15] However, microscopic evidence suggests that in vitro and in vivo grown structures are slightly different and hence the self-assembly is expected to be considerably more sophisticated than initially believed.[16]

As extracted from these investigations, the complexity and multiple levels of hierarchy occurring in such biological systems bring to light that cooperativity is a prerequisite to accomplish highly-ordered functional self-assembled structures with applications in various fields ranging from optoelectronic materials to biomedicine.

2. Cooperativity in Supramolecular Polymers

According to the original definitions of cooperativity,[2] most examples of cooperative supramolecular polymers are generally created by monomeric units that are capable of establishing multiple (various kinds of) non-covalent interactions in an orthogonal fashion while minimizing the possible repulsive interactions that can restrict their supramolecular growth. An exception to this rule are purely hydrogen bonding systems, which on their own represent the driving force for the creation of supramolecular systems based on *cooperative hydrogen bonds*. The singularity of hydrogen bonds originates from their complex nature, whose characterization demands the contribution of different interaction types: electrostatics, polarization, van der Waals and covalency.[17-19] The principles of the cooperative effect in hydrogen bonded supramolecular systems have been reviewed by Meijer and co-workers[20] and its presence and origin described in several publications.[21-33] In these systems, cooperativity has been attributed to entropic reasons due to a lower entropy demand for the association of a monomer to a polymeric structure as for the dimerization of two monomeric units, as well as enthalpic contribution due to several electronic effects, namely long-range dipole-dipole interactions, polarization effects and resonance-assistance.[20]

Supramolecular polymers (SP)[34] can be distinguished depending on the mechanism of their formation into three categories: isodesmic, cooperative and ring-chain polymerization processes. The mechanisms of supramolecular polymerization and their thermodynamic aspects have been extensively described in various reviews by the groups of Moore,[35] Würthner[36] and Meijer[20] and therefore we will not cover these concepts in detail in the present work, but just a brief explanation. Ring-chain supramolecular polymerization is characteristic for ditopic monomeric units in which equilibrium between linear and cyclic counterparts exists.[20] As this mechanism is the least frequently found in artificial systems, in the following we will primarily focus on the isodesmic and cooperative mechanisms. The isodesmic process is comparable to step-growth polymerization and all events of the self-assembly process are characterized by the same value of association constant regardless of the size of the aggregates.[20,35,36] On the other hand, the cooperative (or nucleation-growth) mechanism is a two state process in which the formation of a thermodynamically unfavorable species composed of a limited number of monomeric units (nucleation) is followed by a more favourable elongation step characterized by a much larger value of binding constant (Figure 2a). The result is the formation of self-assembled structures with a high degree of internal order compared with the isodesmic counterparts which give rise to random-coil supramolecular polymers without internal order. To discriminate both self-assembly mechanisms a careful plan of representative studies is important.[37] First, the system under investigation should exhibit a property that changes with concentration, temperature or solvent ratio. Usually this property is the UV/Vis light absorption, Cotton effect or ^{1}H NMR chemical shifts, although other features of the system such as changes in viscosity, IR bands or fluorescence intensity to name some have been also examined. An overview of the guidelines and different experimental and computational techniques that are used to investigate self-assembly mechanisms are covered in a recent concept article from the groups of Balasubramanian and George.[38] Ideally, it should be possible to monitor a complete transformation from monomeric to fully aggregated species in the course of temperature- or concentration-dependent studies. If this is the case, the parameter α_{agg} (fraction of aggregated species) can be accurately derived. This parameter varies between 0 and 1 depending on whether all monomeric units are in a molecularly dissolved ($\alpha_{agg} = 0$) or an aggregated state ($\alpha_{agg} = 1$), respectively. The plot of α_{agg} against concentration or temperature will subsequently define a curve, whose shape will determine the self-assembly mechanism (Fig. 2b). Sigmoidal curves are usually regarded as non-cooperative, as the transition from the monomeric to the aggregated state occurs in a stepwise fashion (Fig. 2b).[20,34-36] Highly-cooperative systems, however, are characterized by much sharper and asymmetric curves showing an all-or-nothing behavior (Fig. 2b).

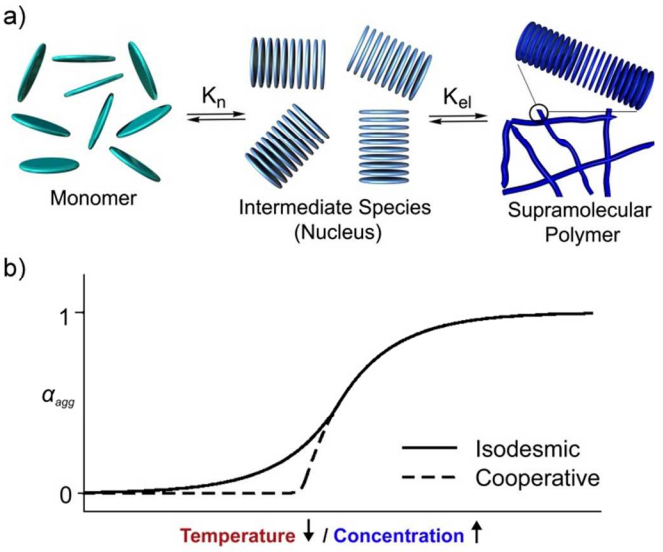

Fig. 2 a) Schematic representation of the supramolecular cooperative growth following the nucleation-elongation pathway, ~~characterized by either a nucleus of variable size or of dimeric structure~~. b) Plot of α_{agg} against increasing temperature and decreasing concentration, respectively giving rise to characteristic curves corresponding to an isodesmic or cooperative growth. Reproduced with permission from refer. 37 (© Wiley VCH).

Various thermodynamic models have been used to fit the resulting cooperative curves. From among several models developed by different authors, four of these are largely used by the scientific community to analyze self-assembly mechanisms depending on whether the data are based on temperature- or concentration-dependent studies (Fig. 2a). All models have in common that they assume an initial, unfavorable nucleation step characterized by a relatively low association constant. Once this step has been overcome, the elongation into extended supramolecular polymers occurs in a highly favorable fashion, as described by much greater binding constants.

The model for *thermally activated equilibrium polymers* applied to temperature-dependent measurements was described by van der Schoot.[20,39-41] In this model, a monomeric activation step occurs that is characterized by the dimensionless equilibrium constant K_a. The elongation temperature T_e divides the self-assembly into the nucleation regime (above T_e) and the elongation (below T_e). The elongation growth is characterized by the dimensionless equilibrium constant K_e and the temperature-independent elongation enthalpy ΔH_{el}.

Likewise, the more recent model developed by ten Eikelder, Markvoort and Meijer also describes a temperature-dependent polymerization growth.[42,43] For this analysis, they assume a nucleus that consists of two subunits formed in an unfavorable dimerization event described by K_2. After this species is formed the elongation can start with a much greater binding constant K. By applying this model to temperature-dependent data, one can define the nucleation (ΔH_{nuc}) and elongation (ΔH_{el}) enthalpy, the entropy ΔS and the elongation temperature T_e. With these thermodynamic parameters one can calculate the equilibrium constants K_2 and K that define the cooperativity factor σ as K_2/K.

The general model concerning concentration-dependent cooperative processes was reported by Goldstein and Stryer.[20,44] This model considers the appearance of a nucleus of variable size s that is formed in an isodesmic fashion with K_n. After this initial event, the polymer grows with an equilibrium constant K and σ is again defined as K_n/K. However, for the growth the *cumulative cooperativity* ω ($\omega = \sigma^{s-1}$) is of importance since the polymerization depends not only on σ but also on the nucleus size s. Therefore, fitting allows to define the *cumulative cooperativity* ω.

A more simplified model for concentration-dependent studies represents the K_2-K model that specifies the nucleus as dimeric assembly characterized by a dimerization constant.[20,45] Fitting the concentration-dependent data to the best match with this model allows the estimation of the cooperativity factor σ, the nucleation (dimerization) and elongation constants.

The main focus of this review will be to discuss various strategies that have been exploited in the literature to create cooperative supramolecular polymers with a high degree of order. We have classified these approaches depending on the non-covalent forces responsible for the observed cooperativity, which will be described as follows.

3. Strategies to create cooperative systems

3.1 hydrogen bonding (and π-π-) interactions

By far, the most commonly used approach to construct highly ordered supramolecular polymers has been focused on systems that self-assemble through cooperative hydrogen bonding interactions and combinations of hydrogen bonding and π-π-interactions, as described in various reviews. [20,38]

In their seminal work from 2006, the group of Meijer reported on the hierarchical self-assembly into fibers by following a nucleation-growth mechanism.[40] The oligo(*p*-phenylenevinylene) (OPV) derivatives (**1**-**3**) feature a ureidotriazine moiety on one side and a peripheral trialkoxy group on the other edge of a central aromatic OPV unit decorated with chiral alkyl chains. This molecular structure allows the formation of dimers by four hydrogen bonding interactions between the complementary ureidotriazines.

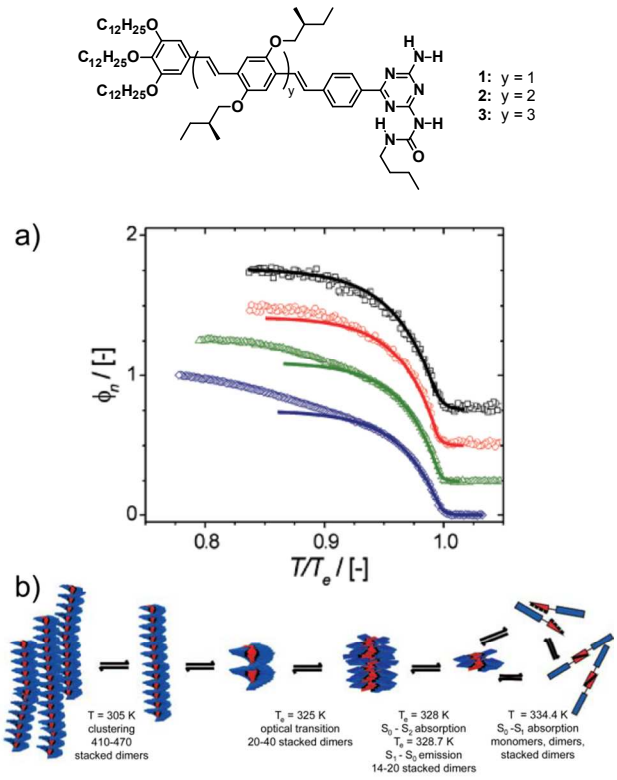

Fig. 3 a) Normalized CD intensities (ϕ_n) monitored at λ = 466 nm upon cooling for four concentrations of **2** in dodecane (symbols) and one-parameter fits to the data (lines). A vertical offset of the curves of 0.25 is applied for reasons of clarity. b) Schematic representation of the hierarchical self-assembly of **2** in solution. Reproduced with permission from refer. 40 (© AAAScience).

Earlier studies on these systems presented the formation of dimeric species in chloroform while in dodecane two different states were detected, namely monomeric species or dimers at high temperature that can further aggregate at low temperature into helical stacks, as observed by UV/Vis, fluorescence and CD studies.[46,47] Regarding the aggregation process, dimerization of the monomers through hydrogen bonding most likely leads to a preorganization of the system in such a way that the overlap of the π-surfaces within the stacks is maximized, thus facilitating the further growth of the system in apolar solvents. More detailed temperature-variable investigations in dodecane revealed a cooperative denaturation for the chiral stacks whose stability depends on the length of the conjugated core since stronger π-π-interactions result in higher melting temperatures.[47] The fibrillar arrangements could further be characterized by SANS and AFM[47] and the dimeric monolayers of OPVs by STM measurements.[48]

As shown in Fig. 3a, analysis of temperature-dependent CD measurements of **2** in dodecane at different concentrations reveals for all of them a clearly non-sigmoidal curve, whose detailed study allows a division of the helical aggregation process into hierarchical steps.[40] It could be demonstrated that the self-assembly can be described by the theory for *thermally activated equilibrium polymerization* that was developed by Oosawa-Kasai and modified by van der Schoot.[39,49] Here, the pathway from isodesmic nonhelical assembly to non-isodesmic helical assembly is characterized by an equilibrium between nonhelical and helical structures of a critical size. Applying this model to the CD curves affords a perfect fitting for the lowest concentration and confirms that the helical aggregates do not exist until the temperature falls under the corresponding (concentration-dependent) elongation temperature T_e. However, for higher concentrated samples the data obtained at lower temperature could not be described by the fitting curve for one-dimensional aggregation that could be assigned to a clustering of the stacks. This could be characterized as isodesmic process and AFM revealed a more pronounced clustering effect at higher concentration. This process represents the last step of the aggregation cascade that can be split into several stages (Fig. 3b). From high temperature, the monomeric species self-assemble into hydrogen-bonded dimers that ~~initially form a pre-nucleus and~~ subsequently assemble upon cooling into small stacks of around 15 dimers in an isodesmic fashion. Upon further cooling (T_e = 328K), the molecules in the stack adopt a higher ordering that is characterized as cooperative transition. Subsequently, a cooperative helical switching occurs in which the preaggregate transforms into an initial chiral species. The average degree of polymerization at this elongation temperature could be determined for **2** to 17 to 41 dimers which fits well with the calculated number of 15 to 30 stacked dimeric units required for one helical pitch. Afterwards, the initial chiral stack can grow into extended helices following a cooperative mechanism.
The elongation temperature T_e depends on the length of the conjugated system of the molecules, with lower temperatures for smaller aromatic surfaces. Not only the conjugated π-surface but also solvent changes affect the T_e values, showing the dependence on the length of the hydrocarbon as well as on the number of carbon atoms of the solvent, i.e even-odd effect. This impact could also be observed for the binding constant and the number of dimers in the aggregates, indicating that the solvent molecules oriented at the periphery of the aggregates play an important role in the self-assembly process.

In a further example, the same group synthesized a related OPV system (**A-OPVUT**) with four aromatic rings bearing achiral linear substituents and an ureidotriazine end group.[50] Chirality in the system was generated upon addition of chiral (*R*)- or (*S*)-citronellic acid (CA) molecules in MCH, giving rise to mirror-image CD spectra depending on the chiral additive. The key role in generating chirality was attributed to hydrogen-bonded linking of the chiral CA guests to the ureidotriazine groups of the gelator. Interestingly, the self-assembly of the 1:1 (**A-OPVUT:CA**) complex also occurs in a cooperative fashion, similar to that of individual OPV.

More recently, De Greef, Meijer and coworkers revealed through an exciting example two distinct pathways for the aggregation of a (*S*)-chiral OPV into thermodynamically favoured M-SOPV or kinetically favoured P-SOPV aggregates.[51]

Benzene-1,3,5-tricarboxamides (BTAs) are a class of molecules that have been widely investigated by Meijer and co-workers.[52-56] In 2008, they investigated the cooperative self-assembly of two literature-known[57-59] C_3-symmetrical trialkylbenzene-1,3,5-tricarboxamides with a chiral alkyl substituent for (*R*)-**4** and an achiral linear chain for **5**.[41] The chiral derivative (*R*)-**4** aggregates in a highly cooperative fashion in heptane, as observed by temperature-dependent CD measurements (Fig. 4) that give rise to a right-handed columnar architecture based on triple hydrogen-bonding interactions. The stacks at elongation temperature (T_e) could be defined to consist of at least 100 discotic molecules that are extended to more than 10000 subunits upon cooling to room temperature. An abrupt change in the degree of aggregation was also observed for (*R*)-**4** in temperature-dependent UV studies. Hence, it was possible to describe the spectral changes by the nucleation-elongation model of van der Schoot[39] showing that the CD studies for **4** are in good agreement with the UV data.

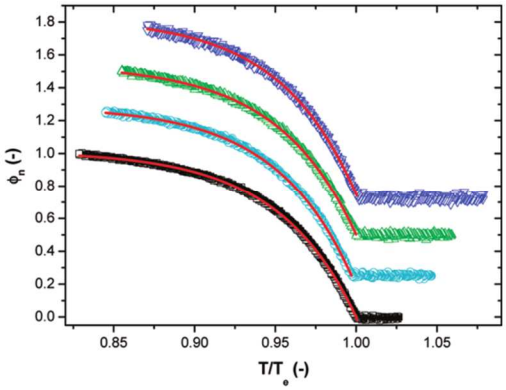

Fig. 4 Degree of aggregation with fitted (red line) elongation regime as a function of temperature for solutions of (*R*)-**4** in heptane, for different concentrations. The curves are shown with a 0.25 offset for each next concentration and as a function of the normalized temperature T/T_e. Reproduced with permission from refer. 41 (© American Chemical Society).

Likewise, the spectral data for the achiral counterpart **5** revealed a cooperative aggregation mechanism and suggested that it also exists as helical stacks but without a distinct helicity, resulting in a CD silent spectrum. These helical structures of **5** further interact laterally at lower temperature inducing a slight deviation from the one-dimensional fitting. A direct comparison shows that the thermodynamic parameters for the cooperative processes of (*R*)-**4** and **5** significantly differ, with a lower cooperative effect and a reduced aggregation tendency for **5**. Sergeant-and-soldiers studies show that the presence of only 4% of the chiral sergeant *(R)*-**4** in a heptane solution of **5** is enough to reach maximum handedness in CD experiments.

Related investigations on this system take a closer look on the temperature dependence of the strong chiral amplification in terms of the helix reversal penalty and the mismatch penalty.[60]

In 2011, the authors moved a step forward towards more complex systems by designing a ditopic BTA derivative **6** whose cooperative self-assembly can be controlled by the addition of an N-methylated BTA **7** as monotopic chain stopper.[61] The investigated ditopic BTA **6** contains three amide groups stabilizing supramolecular assemblies by hydrogen-bonding interactions while its monotopic counterpart **7** lacks the N-H moiety resulting in a monomeric state in MCH and acetonitrile.

Regarding the binary mixture of both BTA derivatives, the addition of **7** induces a drop in the relative viscosity of a MCH solution of **6** (Fig. 5a) that can be assigned to a shortening of the helical aggregates. However, the affinity of **7** to link to the supramolecular polymers of **6** and thus acting as a chain stopper is relatively low, as indicated by the low association constant for chain termination. This can be explained by considering that monomeric **6** adopts an unfavorable conformation in solution that requires a reorganization of its amide functionalities before making contact with the stacks of **7** by hydrogen bonding interaction. The studies on this BTA system enabled the development of a binary self-assembly model that generally describes cooperative supramolecular polymerization in the presence of a second component that can interact with the monomers and/or polymers (Fig. 5b).

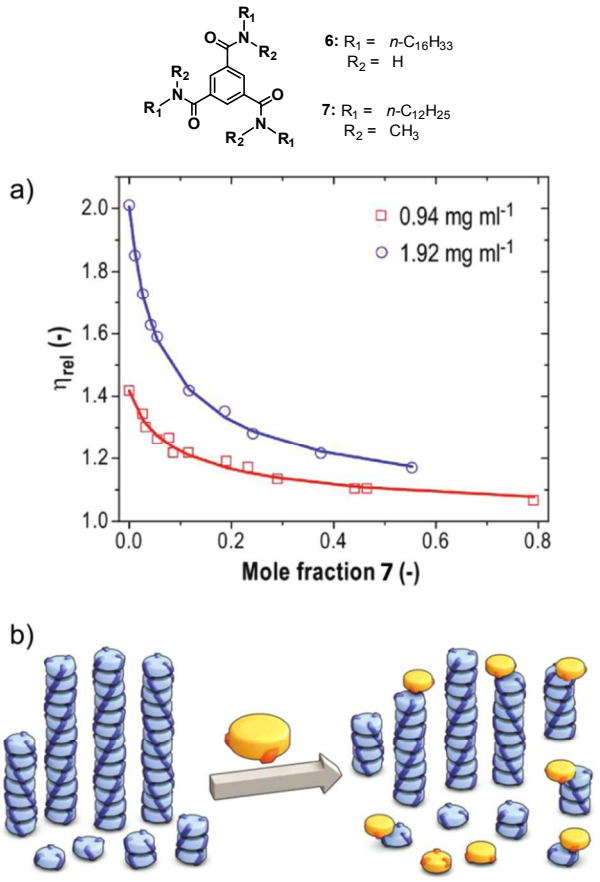

Fig. 5 a) Relative viscosity as a function of mole fraction **7** added for two concentrations of **6** in MCH. b) Schematic representation of the introduction of a monotopic monomer to a ditopic monomer that self-assembles into long 1-D assemblies via a cooperative mechanism. Reproduced with permission from refer. 61 (© American Chemical Society).

After these extensive investigations and characterization of BTAs, Meijer, Palmans and co-workers questioned whether the substitution of the amide by thioamide groups would influence the supramolecular polymerization.[62] To that end, they synthesized new thioamide-based analogs (**8-10**) by treatment of the corresponding BTA precursors with P_2S_5 in hot toluene (Chart 1). The thioamide-based BTAs showed a similar behavior and comparable stability compared to the amide-based derivatives even though differences could be observed concerning their self-assembly.

Chart 1 Molecular structures of Compounds **8**-**10**.

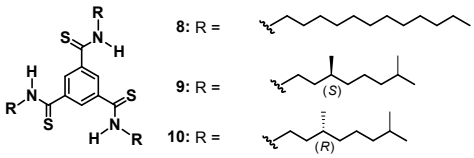

In hydrophobic solvents such as in MCH, the thio-BTAs self-assemble into one-dimensional helical structures that are stabilized by triple hydrogen-bonding interactions, as detected by IR. The melting curves of thio-BTAs extracted from CD showed a clearly non-sigmoidal shape indicative of a cooperative behavior. However, the cooperativity factor σ of 10^{-4} for the thio-BTAs is around two orders of magnitude larger than that of their amide counterparts, revealing that their self-assembly is less cooperative. Since the aromatic unit is equivalent for both molecular classes, this significant difference in the cooperative effect has to be attributed to the hydrogen-bonding interactions between the discotic units. The strength of hydrogen bonding between the thio-amides thus should be weaker than between the amide groups, as could also be identified in dimers of formamide and thio-formamide molecules in 2002.[63]

The following example shows that also hydrogen bonding interactions by themselves can lead to cooperative phenomena, as previously illustrated in the introduction. In this context, Bouteiller and co-workers have extensively focused on the self-assembly behavior of bis-urea derivatives. Initial investigations of branched bis-urea derivative EHUT (**15**) revealed its involvement in the formation of one-dimensional assemblies driven by cooperative hydrogen bonding between two adjacent monomers resulting in viscous solutions in CCl_4 and toluene.[64,65] Due to the unique characteristics of bis-ureas, the studies were extended in 2003 by designing several bis-urea derivatives (**11-21**) with variations concerning the side groups and the position of the methyl group attached to the central phenylene ring in order to investigate how slight structural changes may affect the self-assembly in organic solvents.[66]

Solvent-dependent studies show that the relative viscosity of EHUT (**15**) solutions increases upon lowering the polarity from chloroform to dodecane as a result of stronger hydrogen bonding interactions within the assemblies. Monitoring free N-H vibrations by FTIR studies of EHUT (**15**) and its mono-urea counterparts (**22** and **23**) disclosed the formation of cooperative supramolecular structures in chloroform ($CDCl_3$) (Fig. 6), however the cooperative effect for the mono-ureas is significantly weaker. The cooperative behavior for EHUT (**15**) can be explained as follows: as illustrated in Fig. 6, the association of the two urea functions in one molecule does not occur independently, as for the mono-ureas the 100-fold higher concentration is needed to obtain the transition from monomeric to aggregated species instead of a factor of 2. Furthermore, the significant sharp curve for this transition of EHUT (**15**) could successfully be fitted to the non-isodemic two constant model (K_2, K) giving rise to the thermodynamic K/K_2 value. This parameter also revealed slight cooperativity for the mono-ureas due to polarization effects upon dimer formation, but to a much lower extent. The cooperative behavior of EHUT (**15**) can also be confirmed by comparing the calculated weight and number average degree of polymerization at given concentration of **15** with an isodemic reference compound, that clearly reveals significant differences between the systems.

In 2004, the class of bis-ureas was broadened by designing dissymmetrical systems based on 2,4-toluene diisocyanate showing

that the tendency to self-assemble decreases when the number of hydrogen bonding NH groups is reduced.[67]

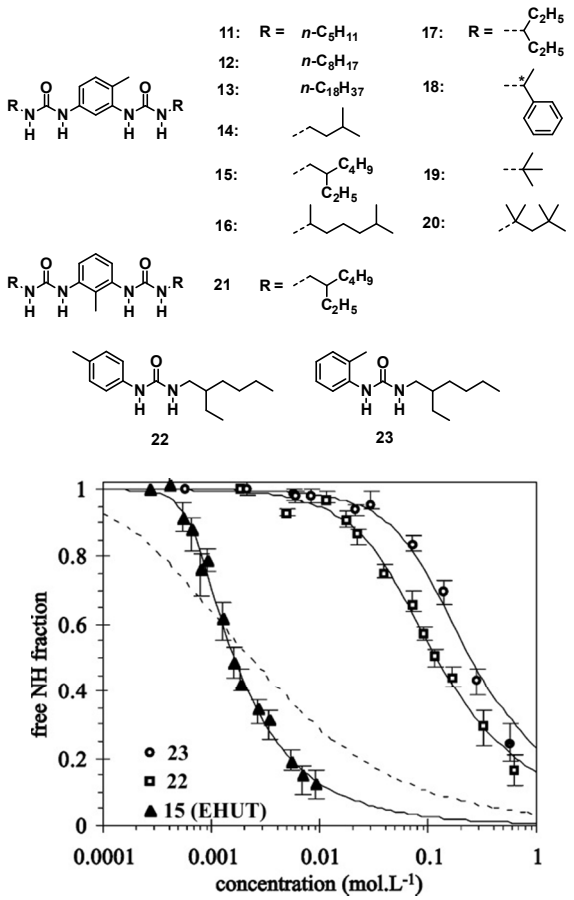

Fig. 6 Fraction of free NH groups of bis-urea EHUT (**15**) and model monoureas **22** and **23**, versus concentration in $CDCl_3$, at room temperature. The full curves are calculated with the non-isodesmic model, the dotted curve is the best fit of the data of **15** to the isodesmic model. Reproduced with permission from refer. 66 (© American Chemical Society).

Following that, further inspection of EHUT (**15**) in toluene showed an unexpected viscosity behavior with a sudden steep decrease around 40 °C, as depicted in Fig. 7.[68] FTIR measurements show hydrogen-bonded urea functions over the complete temperature range, ruling out a disassembly of the sample upon heating. However, slight changes in the N-H vibration band above 40 °C indicated a rearrangement of the urea moieties into less ordered assemblies. This structural change can also be monitored by small-angle-neutron scattering (SANS) studies revealing a morphology transition from thick into thinner and shorter filaments.

All these changes are reversible and occur in a very narrow temperature range of 5 °C suggesting that this molecular rearrangement is highly cooperative. This can be supported by a perfect fitting of the FTIR data to the model for structural transitions in linear assemblies by van der Schoot *et al.*[69,70] providing a considerably high degree of cooperativity (a very low σ value ~ 3.9 x 10^{-5}). This transition can also be induced and tuned upon dilution in toluene, solvent changes and upon mixing of two bis-urea derivatives.

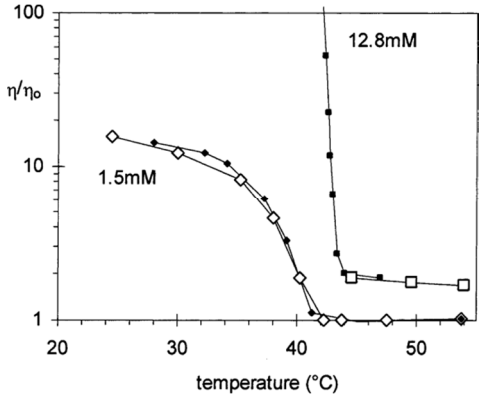

Fig. 7 Relative viscosity of EHUT (**15**) solutions in toluene vs temperature. Heating run (open symbols); cooling run (full symbols). Reproduced with permission from refer. 68 (© American Chemical Society).

After the application of EHUT (**15**) as racemic mixture in various reports, the same authors compared this behavior with the self-assembly of the enantiopure monomers.[71] Circular dichroism (CD) in cyclohexane showed a significant Cotton effect for EHUT-*SS* (**24**) representing the mirror image to EHUT-*RR* (**25**), indicating that the chirality of the side-chains dictates the handedness of the self-assembled system (Fig. 8).

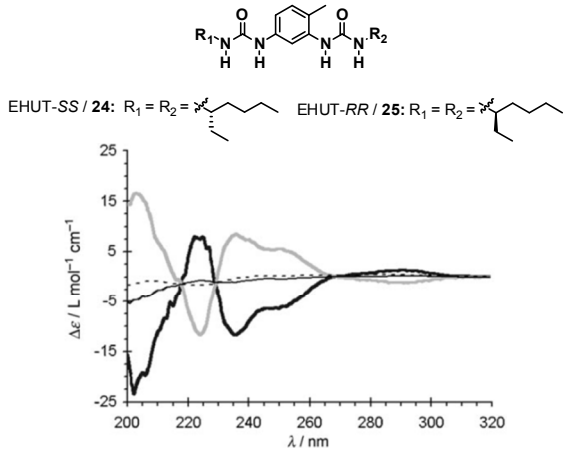

Fig. 8 CD spectra of 1 mM solutions in cyclohexane of: EHUT-*SS* (**24**) at 20°C (bold black line); EHUT-*RR* (**25**) at 20°C (bold grey line); EHUT-*SS* (**24**) at 60°C (black line); EHUT-*rac* (**15**) at 20°C (dashed black line). Reproduced with permission from refer. 71 (© Wiley VCH).

Majority-rules experiments showed that a distinct handedness, which was absent for individual EHUT-*rac* (**15**) solutions, can be induced upon adding a chiral counterpart in a slight enantiomeric excess without influencing the cooperativity of the system. Moreover, the dissolution of EHUT-*rac* (**15**) in chiral solvents (*S*)- and (*R*)-limonene also showed the corresponding Cotton effect indicating that the chiral solvent molecules can act as chiral regulator for the helical assemblies.

Recently, the same group presented a theoretical analysis that enables an improved quantitative measurement of weak non-covalent interactions in solution based on the cooperatively self-organizing bis-urea system as a platform. [72]

The group of F. Würthner has widely studied the self-assembly of perylene bisimides (PBIs).[36,73-76] In 2007, they reported a tetra-bay-substituted perylene bisimide (PBI) **26** that self-assembles in methylcyclohexane (MCH) into J-aggregates exhibiting a fluorescence quantum yield near unity.[77] This novel, slipped aggregation pattern originates from the molecular design of this PBI. The sterically demanding bay-substituents induce a twist of the aromatic PBI core assisted by terminal trialkoxyphenyl groups and a linear arrangement of the dyes is accomplished by hydrogen bonding interactions. The result is the formation of helical fibers in nonpolar solvents, as confirmed by UV/Vis, FTIR and ^{1}H NMR measurements as well as microscopic studies.

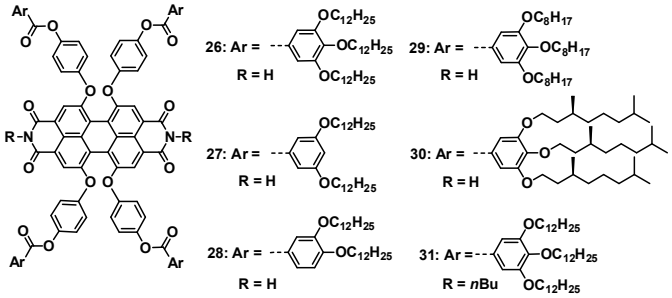

Besides PBI **26**, a second PBI reference compound (**31**) was synthesized that bears a *n*-butyl chain at the imide position. Based on that, this derivative was unable to stabilize self-assembled structures by hydrogen bonding interactions.[45,77] Studies in MCH proved that **31** existed in a molecularly dissolved state at 10^{-5} M and forms only dimeric species upon increasing the concentration, instead of further growing into extended aggregates. Futhermore, the investigations on the core-twisted PBI motif were extended by synthesizing four more derivatives (**27**-**30**) that differ in the number, length and nature (chiral and non-chiral) of the alkoxy bay substituents.[45]

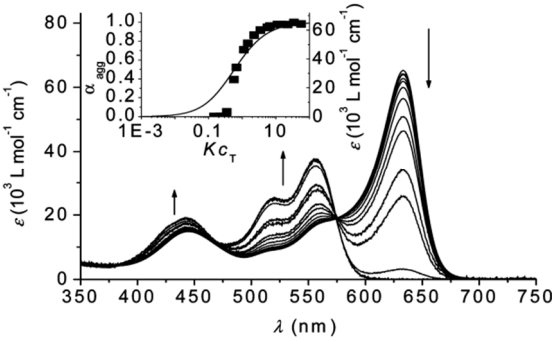

Fig. 9 Concentration-dependent absorption spectra of chiral **30** in MCH (c = 7.3 x 10^{-5} to 1.9 x 10^{-7} M). Arrows indicate the spectral changes with decreasing concentration. (Inset) Change of absorption at λ = 633 nm (black squares) with decreasing concentration; the curve shows the resulting fit calculated according to isodesmic model. Reproduced with permission from refer. 45 (© American Chemical Society).

All investigated PBIs (**27**-**30**) show comparable spectroscopic characteristics with a strong J-aggregation tendency in MCH, similarly to the previously reported example **26**. The aggregation strength for the self-assembly in MCH at 10^{-5} M was largely influenced by the side chains attached to the bay substituent. Unfortunately, stable aggregation down to a concentration of 10^{-8} M precludes further characterization of the aggregation mechanism of **26**-**29** by concentration-dependent measurements. However, the branched alkyl chains of chiral **30** cause a reduced aggregation tendency enabling a further characterization of the system. The spectra from 10^{-5} to 10^{-7} M in MCH (Fig. 9) showed a similar behavior than the temperature-dependent studies, indicating that the complete transition from aggregated to monomeric species can be monitored. The plot of α_{agg} against Kc_T revealed a clearly non-sigmoidal shape, characteristic of a cooperative process.

Applying the K_2/K nucleation-elongation model to the spectral data enabled a manual fitting for the best match with σ values in the range of 10^{-5} to 10^{-6}, corroborating a highly cooperative process. The binding constant K_2 for the unfavorable dimerization step of **30** could be defined to be 13 ± 11 M^{-1} while the subsequent elongation constant K has a remarkably higher value of 2.3 ± 0.1 x 10^6 M^{-1} due to the interplay of π-π- and hydrogen bonding interactions between the cooperatively aggregating molecules. These attractive forces lead for chiral **30** to the creation of helical systems in MCH as indicated by the CD spectra.

Comparing the cooperative self-assembly of **26**-**30** with the dimerization of imide-substituted **31** which lacks contribution from hydrogen bonding interactions, one can clearly recognize that the cooperativity of the PBI aggregation process is induced by simultaneous participation of π-π- and hydrogen bonding interactions in MCH.

Recently, Würthner, Lochbrunner and co-workers investigated a structurally related core-twisted PBI **32** substituted with butylphenoxy substituents at the bay and bulky benzamide groups at the imide position.[78] The amide spacers enable hydrogen bonding that support the aromatic attraction between the PBI cores giving rise to a strong aggregation in MCH. This aggregation process shows a biphasic temperature dependence for **32**, as visualized by fluorescence studies (Fig. 10a). Upon decreasing the temperature from a fluorescent, molecularly dissolved state (90°C) to 40°C a simultaneous red-shift, decrease and broadening of the emission band can be detected, accompanied by a decrease of the fluorescence quantum yield by a factor of 2.

However, upon further cooling to room temperature the emission is again blue-shifted and largely recovered with a significant increase in quantum yield. These changes, supported by quantum chemical calculations could be attributed to the presence of two distinct self-assembled species, characterized by an initial "aggregation-induced quenching" followed by an "aggregation-induced emission" upon enlargement of the aggregated system. A comparable, biphasic process could also be observed for variable-concentration studies. Combining all spectral features, the authors concluded that at intermediate temperature or concentration, dimers with an H-type arrangement exist that are stabilized by hydrogen bonding interactions, making their formation energetically favorable as evidenced by the high dimerization constant, K_D (Fig. 10c). This arrangement precludes the enlargement of the structure and consequently at lower temperature or higher concentration a second, sterically less restricted J-type dimer is formed. This new, laterally-shifted orientation results in a reduced stabilization by hydrogen bonds and π-π-contacts as it becomes apparent in the low association constant K_D'. However, it facilitates the subsequent elongation of the system into J-type aggregates characterized by a binding constant $K_A >> K_D'$. Due to the biphasic behavior, it is not possible to apply the data to a distinct aggregation model. However, regarding only the J-type aggregate pathway, the comparison of the equilibrium constants ($K_A >> K_D'$) as well as the plot of the fraction α against the total concentration (blue line in Fig. 10b), characterized by an abrupt increase in J-aggregated species upon reaching a certain concentration, is clearly indicative of a cooperative process.

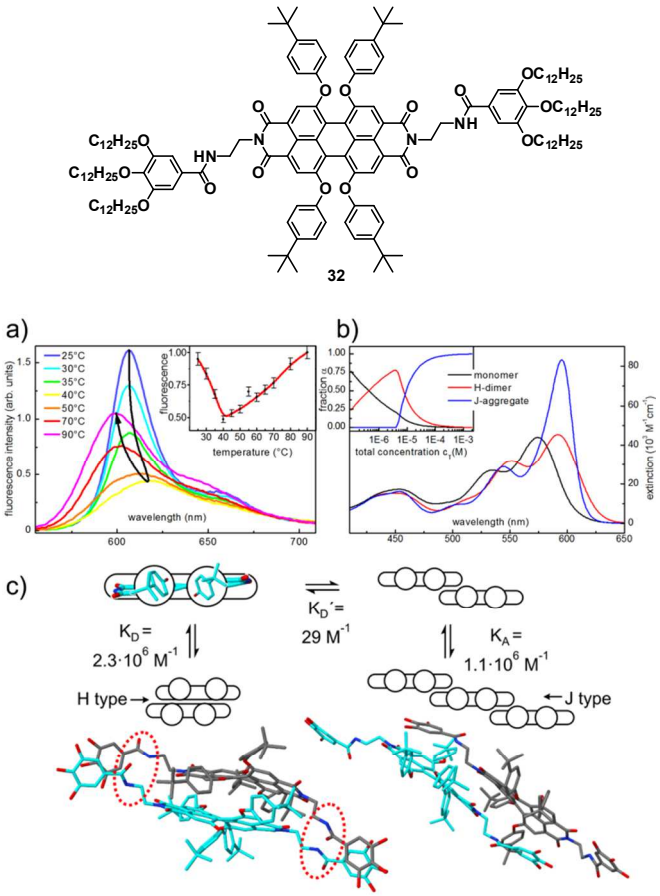

Fig. 10 a) Temperature-dependent fluorescence spectra and normalized integrated yield (inset) of PBI **32** in MCH at c = 0.02 mM. b) Spectra of the monomer, favored H-dimer, and larger J-aggregates extracted from the aggregation model. The inset shows the fraction of monomers, molecules in the favored H-dimer, and molecules in J-aggregates as a function of the total dye concentration. c) Proposed aggregation model and calculated structures of the favored dimer and the dimer acting as nucleus for the aggregates. Reproduced with permission from refer. 78 (© American Chemical Society)

Yagai and co-workers synthesized in 2011 monotopic melamines with two PBI chromophores attached via an alkyl spacer at the secondary amino groups and achiral (**35**) or chiral ((*S*)-**33** and (*R*)-**34**) substituents at the tertiary amino group.[79] The focus of their work is the investigation of a 3:1 mixture of functionalized melamines and tritopic cyanuric acid (CA).

This complex (**33_3*CA** to **35_3*CA**) is stabilized by multiple hydrogen bonding interactions between a central CA unit and the melamine moieties of three linear compounds (**33-35**) supported by π-π-interactions between the aromatic PBI surfaces creating supramolecular disks (Fig. 11). The self-assembly of these complexes of (*S*)-**33** in MCH was studied by CD, obtaining the saturation in CD intensity at 1:3 ratio when (*S*)-**33** was titrated with CA. The same stoichiometry was observed for experiments with the enantiomer (*R*)-**34** giving rise to signals in the CD spectra of opposite sign. Due to the discotic 3:1 geometry of one complex, it is suggested that the periphery of the helix consists of three rotating stacks of interacting PBI pairs while the CA subunits constitute the central core leading to an embedding of the chiral substituents in the inner part of the arrangement (Fig. 11). The π-π-interaction between PBI units is confirmed by Flash-photolysis time resolved microwave conductivity measurements affording mobility values indicative of extended π-stacks. The dense helical architecture results for **33_3*CA** ([(*S*)-**33**] > 20mM) in the formation of highly viscous solution in MCH that finally turns into gel after some weeks of aging. The gel morphology consists of fibers with a uniform width of 10 nm and a height of 2nm that further organize into thicker bundles, as visualized by AFM and TEM imaging of a diluted sample. This behavior differs from that of the individual ligand (*S*)-**33** that is not able to form gels in these aliphatic solvents.

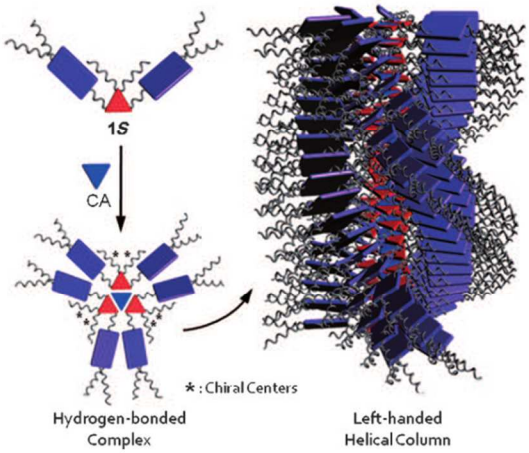

Fig. 11 Schematic representation of a proposed helical columnar structure formed from hydrogen-bonded complex **33_3*CA**. Reproduced with permission from refer. 79 (© Wiley VCH).

Temperature-dependent CD studies of a diluted solution of **33_3*CA** in MCH revealed a non-sigmoidal melting curve, clearly indicating a cooperative aggregation that is driven by π-stacking and hydrogen-bonding interactions. Although the authors did not further focus on the cooperative nature of the self-assembly process, this exciting behavior points out, along with recent examples from the groups of Würthner[45,80] and Meijer[81] that the self-assembly of PBIs is not exclusively limited to their usual non-cooperative aggregation mechanism.[76,82,83]

These studies have been followed by other hydrogen bonded systems based on various classes of dyes.[84-87] In an interesting example, the creation of columnar structures by complex formation of a monochromophoric CA-functionalized perylene bisimide derivative and melamine was explored.[88] Concentration dependent absorption studies of a 1:1 mixture in chloroform showed a cooperative process when the data was fitted to a nucleation-elongation model[35].

Sánchez and co-workers have extensively focused on the self-assembly of oligo(phenylene ethynylenes) (OPEs).[89-94] 2011, they

reported the cooperative self-assembly of an achiral (**36**) and two chiral ((*S*)-**37** and (*R*)-**38**) C_3-symmetrical OPE-based trisamides into helical structures.[95]

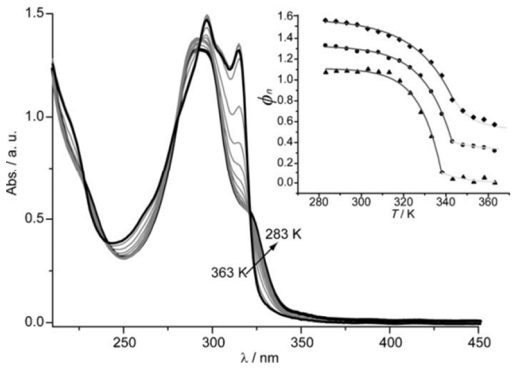

Fig. 12 Temperature-dependent UV/Vis spectra of **36** (MCH, c = 1 x 10^{-5} M, 363 to 283 K, at intervals of 5 K). The inset shows plots of the molar fraction of aggregates versus temperature fitted within elongation (dark grey) and nucleation (light grey) regimes (squares = **36**, dots = (*S*)-**37**, triangles = (*R*)-**38**). Curves in the inset are depicted with a 0.3 offset. Reproduced with permission from refer. 95 (© Wiley VCH).

The helical nature of the assemblies of **36-38** in MCH could be identified by FTIR and further characterized as right-handed helix in case of (*S*)-**37** and an arrangement of opposite handedness for (*R*)-**38**. Temperature-dependent CD studies reveal that these solutions become CD inactive above 363K, however upon cooling helicity is recovered and abruptly grows in a non-sigmoidal fashion. The suggested cooperative nature of the aggregation process can be confirmed by temperature dependent UV/Vis studies in MCH (Fig. 12) revealing a transition from monomeric to aggregated species upon cooling (from 363 to 283 K) that fits perfectly to the nucleation-elongation model proposed by Meijer and coworkers.[40,41,60,96]

The average number of molecules in the stacks at T_e could be defined to be around ten, which perfectly matches with the stabilization energy per subunit for a helical stack of **36** that saturates around 8-12 molecules as suggested by DFT calculations. This aggregate size at elongation temperature is around ten times smaller than that found for literature-known BTAs,[41,60,96] as e.g. previously described for molecule (*R*)-**4** that forms stacks of around 100 subunits at T_e.[41] This difference indicates that the extension of the π-framework from BTAs to the OPE-based trisamides favors the activation step and results in a reduction of the aggregate length at T_e.

The thermodynamic parameters extracted from UV/Vis are in good agreement with those of the CD experiments offering a high cooperativity for (*S*)-**37** and (*R*)-**38** (K_a of 10^{-4}) and a slightly lower cooperative effect for the achiral substituted **36** (K_a of 10^{-3}).[95] The origin of cooperativity in the helical architectures was attributed to the interplay of π-π-interactions between the aromatic cores and triple hydrogen bonding between the amide groups, as identified by concentration-dependent ^{1}H NMR, FTIR studies and DFT calculations.

In a further work, the same authors extended their studies on OPE-based trisamides (**39-40**) as well as alkoxy-amides (**41-43**).[97] For both classes, derivatives with only one kind of substituent as well as asymmetrical derivatives with different substituents in the molecular structure were synthesized and their ability to form chiral objects was investigated.

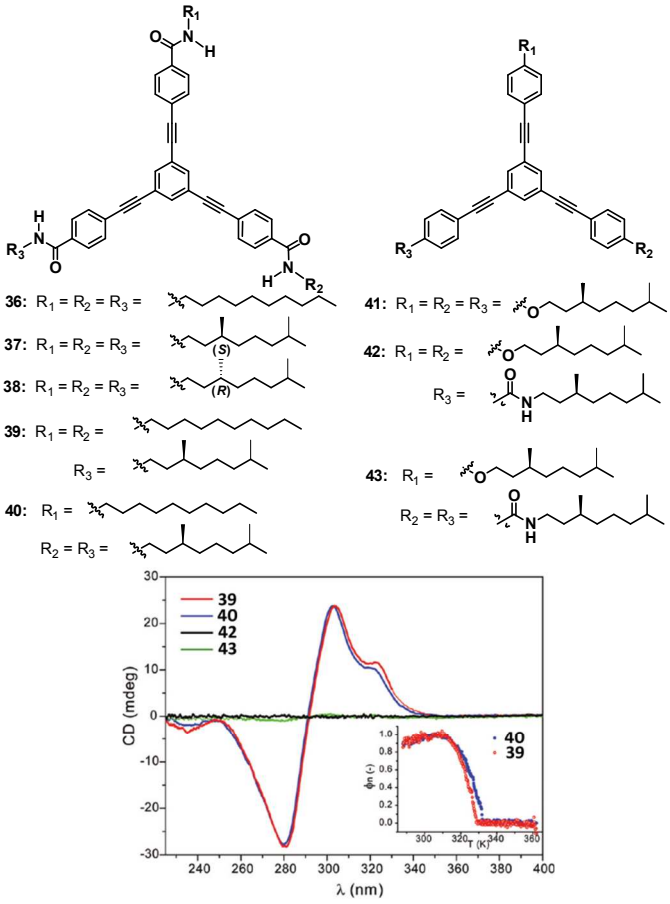

Fig. 13 CD spectra of **39** (red line), **40** (blue line), **42** (black line) and **43** (green line) (MCH, c = 1.5 x 10^{-5} M). (Inset) Non-sigmoidal melting curves of **39** (red) and **40** (blue), 363 to 288 K, at intervals of 0.5 K/min. Reproduced with permission from refer. 97 (© American Chemical Society).

Both unsymmetrical chiral compounds **39** and **40** show a very similar behavior as previously reported for symmetrical systems **36** (achiral) and (*S*)-**37** (chiral). The CD spectra of **39** and **40** show the presence of right-handed helical structures (Fig. 13) whose formation can be accurately described by the cooperative nucleation-elongation model by van der Schoot.[40,41] Remarkably, the helicity in aggregated **40** shows that the presence of only one stereogenic center in the molecular design can dictate the handedness of the helical systems. However, the helical structures formed by asymmetrical monomers **39** and **40** are less stable than those of their symmetrical counterparts **36** and (*S*)-**37** due to weaker stabilizing interactions generated between the dissimilar achiral and chiral side chains.

The important contribution of triple hydrogen bonding interactions to induce aggregation into helical arrangements can be confirmed by investigating related OPE derivatives **41-43** in which one to three amide functionalities are replaced by ether groups. This structural variation precludes the stabilization by hydrogen bondings and thus the ability to form helical arrangements, as demonstrated by the absence of any CD signal.

However, also for non-helical but chiral **43** the self-assembly into helical architectures can be induced by the addition of helical but achiral **36**. Upon cooling of the molecularly dissolved state a cooperative 1:1 co-assembly takes place, as determined by CD studies and Job's plot analysis. In these assemblies, both co-monomers benefit from this mixing process by a transfer of helicity and chirality, respectively.

In 2013, the comparison of OPE and BTA systems was extended upon regarding the detailed enthalpy and entropy contributions in their self-assembly processes in MCH.[98] In these studies, the thermodynamic parameters for the cooperative self-assembly of derivatives **36-38** and an identically substituted BTA counterpart ((*R*)-enantiomer of molecule **4**), exhibiting a reduced aromatic core, were investigated.
The direct comparison of the thermodynamic data revealed very similar values indicating that comparable supramolecular attraction appears within the structures. This clearly shows that the main contribution to the stability of OPE and BTA assemblies derives from the directional hydrogen bonding interactions and that an enlargement of the π-surface does not account for an increased stability. This can be explained by the fact that only the central rings (included both in BTAs and OPEs) can perfectly overlap resulting in attractive aromatic interactions, as already illustrated in the calculated helical structure reported in 2011.[95]

In a complementary work, Meijer and coworkers described the helical self-assembly of two structurally-related classes of OPE derivatives with C_3- (**44**-**46**) and C_2- (**47**) core symmetry featuring three amide groups and two or three peripheral alkoxyphenyl substituents to enhance the solubility in apolar solvents (Chart 2).[99]

Chart 2 Molecular structures of Compounds **44**-**47**.

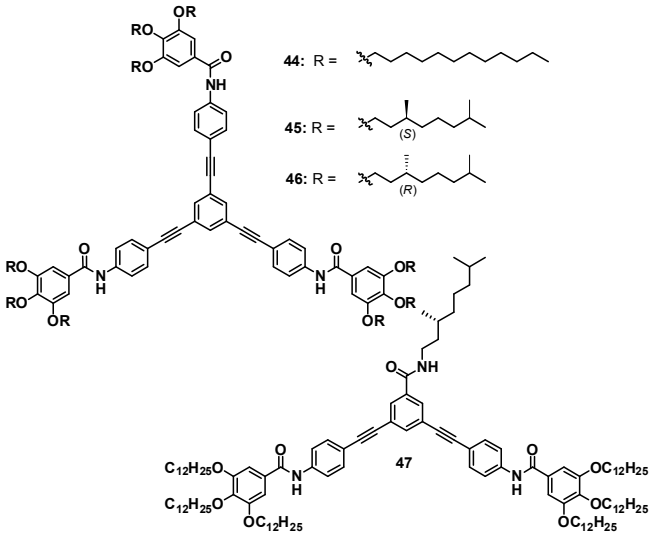

The authors observed that the symmetry of the core has a significant impact on the aggregation process, showing for the C_2 symmetrical discotics a tenfold lower degree of cooperativity as well as lower binding constants compared to the C_3 derivatives.

Sánchez and co-workers presented in 2012 the cooperative aggregation of a chiral linear tetraamide **49** showing an amplification of chirality upon mixing the chiral derivative with a non-chiral counterpart **48**.[100]
CD-experiments of **49** in MCH show a bisignated Cotton effect that disappears at 363 K but shows a non-sigmoidal recurrence upon cooling, indicative of a cooperative behavior (Fig. 14a). The fitting of the extracted melting curve to the nucleation-elongation model[40,41] provides good results demonstrating that the interplay of directional hydrogen bonding between the amides, aromatic contacts between the π-surface and van der Waals interactions between alkyl substituents results in the cooperative formation of helical structures.

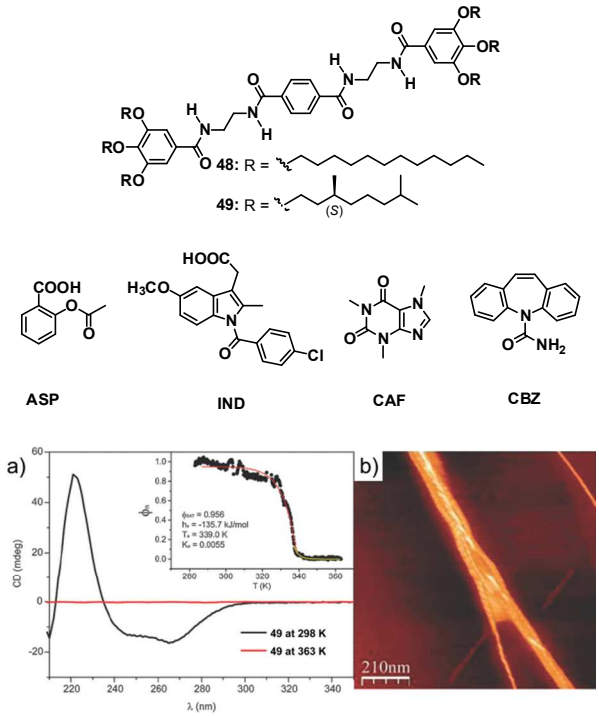

Fig. 14 a) CD spectra of **49** (MCH, 1 x 10^{-5} M). The inset depicts the melting curve from 363 to 283 K at intervals of 1 K/min. Red and yellow lines in the inset are the fits corresponding to the elongation and nucleation processes, respectively. b) AFM height image of the diluted (1 x 10^{-5} M in toluene) gel of **49** onto HOPG (z scale=15 nm). Reproduced with permission from refer. 100 (© Royal Society of Chemistry).

Similarly to **49**, the self-organization of **48** into helical columnar structures results in the formation of colorless gels in toluene. AFM images of these gels formed by **48** and **49** confirm the entanglement of one-dimensional, chiral aggregates into a dense network (Fig. 14b). This gelation ability can be ultimately exploited for the crystallization of pharmaceutical ingredients like **ASP**, **CAF**, **IND** and **CBZ**. The crystals formed therein are easy to isolate and do not show differences in the polymorphic outcome compared to crystals gained in toluene. On the basis of these findings, related organogelators were synthesized by the same group to investigate how structural variations, affecting the number and type of non-covalent interactions in linear molecules, may modify their self-assembly.[101]

The groups of Ghosh[102-108] and George[109,110] have been strongly involved in the investigation of hydrogen bonded driven self-assembled charge-transfer complexes.[111] Similarly, the groups of Ajayaghosh[112-115] and Amabilino[116-119] have extensively studied a wide number of supramolecular systems based on hydrogen bonding. Although the self-assembly mechanism has not been investigated in detail, it is clear that cooperative π-π- and hydrogen bonding interactions are the driving force for aggregate/gel formation.

3.2 π-π- and Metal-Metal interactions

The unique properties of metal complexes have been exploited in various research fields, with particular emphasis on supramolecular chemistry. The ability of metal complexes to form self-assembled structures by various non-covalent interactions often supported by unique metal-metal interactions leads to materials with remarkable optical, electrochemical, redox and other fascinating properties.[120-126] Strong interactions among closed-shell metal ions have been extensively utilized by several research groups to create 1D crystalline or soft materials.[127-130] For instance, trinuclear Au(I) pyrazolate complexes have been reported by Aida and coworkers to form stable organogels that show a luminescence color switch from red to blue to green upon simple addition of silver cations and heating.[131] Interestingly, a structurally related Cu(I) pyrazolate complex was reported that can be applied in security technology for rewritable media. This complex exhibits a dichroic luminescence character that can be controlled by kinetic or thermodynamic self-assembly.[132] The groups of Yam, Che, De Cola and Strassert among others have exhaustively investigated Pt(II) complexes due to their ideal square-planar geometry and intriguing properties, as also described in recent exciting examples.[133-142]

Although extensive efforts have been devoted to the characterization of supramolecular systems based on metal-metal interactions in the last decade, it was not until 2013 when the quantitative contribution of these weak forces to supramolecular polymerization processes was examined.[143]

In this regard, our group reported an OPE-based Pd(II) pyridyl complex **50** that shows a significant color change in MCH from colorless to greenish yellow upon cooling down from a molecularly dissolved (50 °C) to an aggregated state at room temperature. Detailed investigations of this process by temperature-dependent UV/Vis studies (Fig. 15a) revealed the appearance of a red-shifted band at room temperature covering the spectrum up to 470 nm that can be ascribed to cooperative metallophilic interactions between the Pd(II) centers and π-π-interactions between the OPE cores. The cooling curves of **50** (Fig. 15b) possess a non-sigmoidal shape indicative of a cooperative aggregation phenomenon. Fitting these data points to the nucleation-elongation model developed by ten Eikelder, Markvoort, Meijer and coworkers[42,43] gave a perfect match with a significant degree of cooperativity ($\sigma = 3.5 \times 10^{-5}$). Similar results were obtained by concentration-dependent studies and application of the cooperative Goldstein and Stryer[20,44] model confirming the highly cooperative process.

To get closer insight into the quantitative influence of Pd···Pd interactions on the cooperative self-assembly, an OPE derivative **51** was synthesized that exhibits same size and shape as complex **50** but the metal centre is replaced by an alkyne function. Variable-temperature UV/Vis studies show a comparatively slight bathochromic shift of the absorption maximum upon aggregation, clearly indicating that the red-shifted band in case of Pd(II) complex **50** stems from the participation of the Cl-Pd(II)-Cl units in intermolecular bonding. Moreover, the aggregation mechanism of **51** could be characterized as isodesmic, further indicating that cooperativity in the Pd(II) system **50** arises from metallophilic Pd···Pd interactions, most likely also supported by π-π-stacking. This assumption was supported by Density functional theory (DFT) calculations that revealed a simultaneous σ-bond between the Pd centers and two Pd-Cl interactions involving different monomeric units. The increased stability based on these interactions also becomes visible in microscopic studies (AFM) showing extended associates for **50** (Fig. 15c,d) in contrast to the metal-free counterpart **51** that aggregates into considerably smaller and lower-ordered rod-like structures.

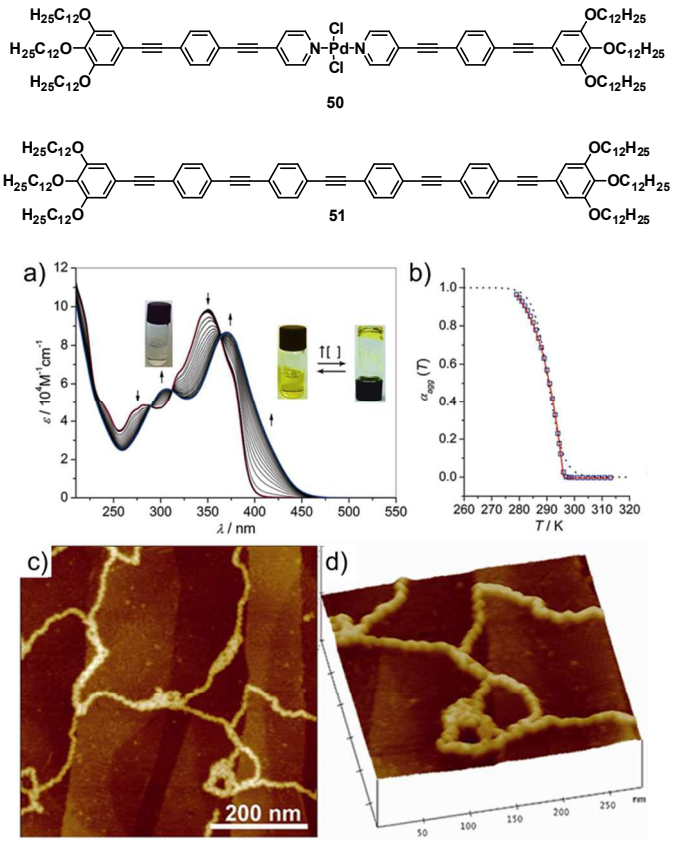

Fig. 15 a) Temperature-dependent UV/Vis experiments of **50** (MCH, c = 1.6 x 10^{-4} M, 343 to 278 K). Arrows indicate the spectral changes upon decreasing temperature. b) Fitting of α_{agg} at 415 nm to the ten Eikelder-Markvoort-Meijer model. c, d) Height and 3D (d) AFM images obtained upon spin-coating a solution of **50** (MCH, c = 8 x 10^{-4} M) on HOPG. Reproduced with permission from refer. 143 (© American Chemical Society).

Recently, the group of Wang reported the self-assembly of rod-like platinum(II) acetylide complexes, containing an amide group with a linear achiral (**52**) or chiral (**53**) alkyl chains, into extended supramolecular aggregates (Chart 3).[144]

Chart 3 Molecular structures of Compounds **52** and **53**

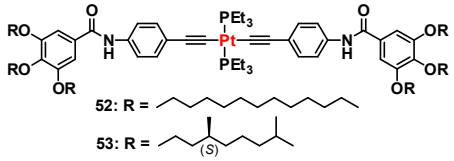

The assemblies of **52** are able to form gels in non-polar solvents accompanied by a gelation-induced emission-enhancement. Detailed ^{1}H NMR studies show that the polymerization is originated from simultaneous intermolecular hydrogen bonding and π-π-interactions between the subunits. Furthermore, the self-assembly of **53** into helical structures was identified as cooperative growth, as could be revealed by the successful fitting to the van der Schoot model[40,41] with a K_a value of 4 x 10^{-4}. However the contribution of metal-metal interactions in the self-assembly of the complexes is not discussed. Although it is known that bulky groups attached to the Pt centers hinder the realization of the metal-metal interactions,[145] it cannot be ruled out that the $Pt(PEt_3)_2$ centers can come close enough to participate in non-covalent interactions.

3.3 Metal-Ligand and π-π-interactions

In the following section, a special kind of cooperative process will be described which stems from the interplay of metal-ligand and intramolecular π-π-interactions that can thus be characterized as "supramolecular chelation based on folding".[146,147]

In this regard, Moore and co-workers investigated the coordination of five mono-functionalized m-phenylene ethynylene (*m*PE) oligomers (**54**-**58**) to a palladium center and the tendency of the resulting complexes to organize in a folded conformation.[146] The authors based their studies on previous investigations by Nelson et al. on the affinity of elongated phenylacetylene oligomers to cooperatively adopt a stable helical conformation by interstrand contacts.[148] Nelson et al were also able to determine the critical chain length for *m*PE derivatives required for helical stability which were at least 7-8 aromatic units per molecule. The oligomer folding was confirmed by the group of Moore in 1999 that presented the fitting to the helix-coil equilibrium model[149] supporting the cooperative folding by intramolecular aromatic stacking and solvophobic effects.[150]

The *m*PE derivatives **54**-**58**, published in 2005 by Moore and co-workers consist of aromatic scaffolds of 1 to 9 rings terminated at one end with a pyridine group as metal ligating moiety.[146]

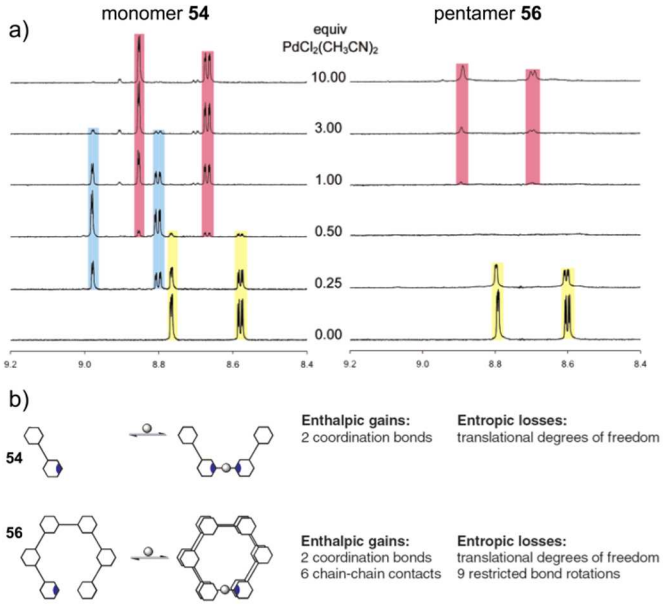

Fig. 16 a) ^{1}H NMR spectra of monomer **54** and pentamer **56** (c = 1 mM) with varying eq. of $PdCl_2(CH_3CN)_2$ in CD_3CN. Resonances colored as follows: free ligand (yellow), 2:1 complex (blue), and 1:1 complex (red). b) Simplified model of the thermodynamics of complexation. Reproduced with permission from refer. 146 (© American Chemical Society).

The coordination to palladium dichloride results in a 2:1 *trans*-complex formation of square-planar geometry. As monitored by ^{1}H NMR studies, the complexation of the monomer **54** and the pentamer **56** with *trans*-$Pd(MeCN)_2Cl_2$ shows distinct differences. The 2:1 complex formed by ligand **54** exists in a still unfolded state while for the complex of **56** a tremendous broadening in the aromatic region clearly indicates a folded conformation (Fig. 16a). These distinct characteristics are consistent with former findings of a critical chain length, indicating that the elongation of the meta-linked aromatic backbone upon coordination of **56** to Pd(II) activates the self-assembly of the 2:1 complex into helices with six repeat units per turn[151]. This folding can partially be rescinded by the addition of an excess of Pd(II), resulting in a reorganization of the ligands into 1:1 complexes that do not reach the required critical length for **54** just as for **56.** Upon closer inspection of the ^{1}H NMR data, a significant difference in the behavior of **54** and **56** becomes noticeable that indicates positive cooperativity for the pentamer. While after addition of 0.5 eq of Pd(II), for **54** the monomeric species, 2:1 and 1:1 complex coexist, in the case of **56** the exclusive formation of the folded 2:1 assembly occurs. Furthermore, in the presence of excess of Pd(II) the 1:1 complex dominates for **54** while the majority of **56** persists in the 2:1 assembly indicating an increased stability of this species. This evidence for cooperativity of **56** was further proven by isothermal calorimetry (ITC) that enables the calculation of the thermodynamic parameters and the association constants for the coordination of the first (K_1) and second (K_2) ligand to the metal center. In contrast to the short oligomers **54** and **55**, a K_2 value greater than K_1 can be defined for the folding species **56**-**58**, indicating a cooperative process, similarly to a chelating effect[152,153] as suggested by the authors.
Regarding the coordination of the second ligand to the Pd(II) center, the enthalpic and entropic contributions revealed significant differences between the oligomers of different length that did not occur for the first step (Fig. 16b). This can be explained by considering that the first coordination step only represents the formation of a new metal-nitrogen bond that is equal for all *m*PEs while the second step includes the second metal-ligand bond formation and the folding of the 2:1 assemblies of different length.

Shortly after these studies, Moore and co-workers investigated similar bis-functionalized *m*PE molecules (**59**-**61**) with two terminal pyridyl groups per molecule.[147]

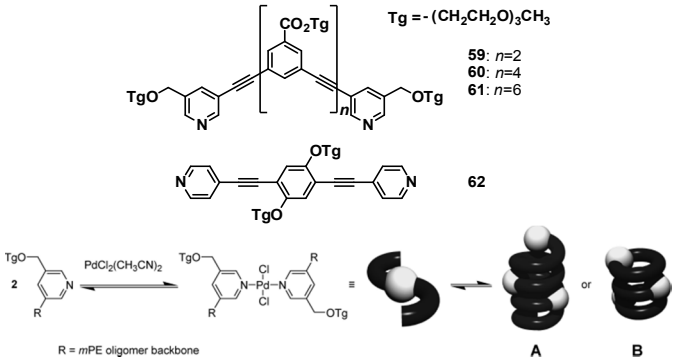

Fig. 17 Palladium-pyridine binding to form a metal-ligand complex followed by subsequent "monomer" additions to form a supramolecular foldamer (A) or a π-stacked columnar polymer (B). Reproduced with permission from refer. 147 (© American Chemical Society)

Similarly to the previous example, the addition of Pd(II) to **59**-**61** resulted in the creation of different supramolecular structures. For the hexameric derivative **60** columnar assemblies were formed. These stacks originate from the isodesmic stacking of 2:2 (**60**:Pd(II)) macrocycles as a result of a perfect fit of the hexamer length into such unstrained cyclic assemblies (Fig. 17). However, the addition of

Pd(II) to a tetramer (**59**) or octamer (**61**) induces polymerization into helical arrangements, described by a nucleation-elongation mechanism involving cooperative ligand-Pd(II) and interstrand π-π-interactions (Fig. 17). Regarding this process, the essential number of coordination steps to reach the suitable nucleus size depends on the oligomer length, since the elongation does not start until the folding of the chain occurs. Similar experiments for a reference compound **62** show that changing the linkage of the oligomer scaffold from *meta* to *para* results in the formation of linear assemblies, now following a non-cooperative growth.
These diverse polymerization mechanisms highlight that the self-assembly of these coordinating oligomers can be controlled by the length as well as the geometry of their aromatic backbone.

3.4 Dipole-dipole/Zwitterionic interactions and other contributions

Dipole-dipole interactions arise from electrostatic interactions of polar molecules due to their ground state dipole moment μ_g. This highly attractive interactions lead to preferred antiparallel arrangements in a dimer species in a so called "sandwich-type" orientation.

A great deal of effort was dedicated by Würthner and co-workers to study the properties and the self-assembly of dipolar merocyanine (MC) dyes.[154-161] In their seminal work of 2003, they described the first example of a hierarchical supramolecular polymer based on MC dyes by synthesizing a bis(MC) derivative **64** whose tridodecyloxybenzyl unit allows its dissolution in a large variety of organic solvents.[162] The behavior was compared with a reference compound **63** featuring a single MC chromophore that is likewise decorated with this solubilizing substituent.
Whereas reference mono-MC **63** self-assembles into dimeric aggregates in nonpolar solvents, a more complex solvent-dependent behavior into different assemblies (dimers and extended H-type species) was observed for the target bis(MC) **64**, as characterized by distinct absorption bands (Fig. 18a). While at 10^{-5} M for a dichloromethane solution a monomer spectra with λ_{max}=570 nm (M band) can be observed, in trichloroethylene the band is hypsochromically shifted to λ_{max}=480 nm, assigned to dimerization of MC units (D band) that results for the bis(MC) in an extended polymer chain. However, upon further decreasing the polarity to tetrachloromethane or methylcyclohexane (MCH), a sharpened and further hypsochromically shifted H-band appears (λ_{max}=447 nm) indicating a further aggregation of the self-assembled strands and revealing different aggregation steps.
These distinct stages of self-assembly are depicted in Fig. 18c: the monomeric bis(MC) **64** initially self-assembles into a one-dimensional strand due to dipolar aggregation of the MC units of one molecule with neighboring dyes. These polymeric assemblies adopt a helical conformation that can further bundle into thicker fibers consisting of six filaments. The subunits in these sophisticated aggregates show an H-type packing in an antiparallel orientation.
Further entanglement of these fibers is responsible for the gelation of MCH at high concentrations and the formation of highly ordered supramolecular structures (Fig. 18b).

To analyze the contribution of dipole-dipole interactions to the supramolecular growth, the same group reported the self-assembly of a related bis(MC) dye series bearing linear (**65**, **66**) or branched alkyl chains (**67**), in which the substitution pattern was changed from *meta*- to *para*.[163]

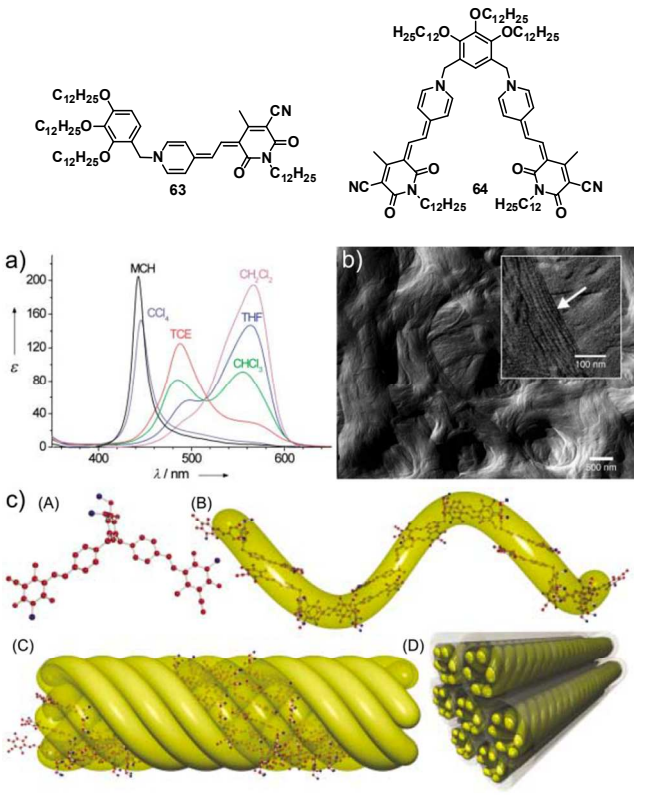

Fig. 18 a) Solvent-dependent UV/Vis absorption spectra (ε in 10^3 $M^{-1}cm^{-1}$, c = 10^{-5}M) of **64** at 293 K. b) Cryo-TEM picture (negative) of a gel of **64** in *n*-hexane (c = 6.5 x 10^{-3} M). c) Model for the hierarchical growth: (A) force-field-optimized molecular structure of **64**; (B) helical supramolecular polymer of **64** formed by dipolar aggregation of the MC units; C) rod-type H-aggregate formed from six helical polymeric strands; D) hexagonal arrangement of the columns. For clarity and ease of calculation, all dodecyl chains have been replaced by methyl groups. Reproduced with permission from refer. 162 (© Wiley VCH).

For **67** the monomeric form dominates over a large concentration range as a result of a high solubility and steric effect introduced by the branched chain. In contrast, molecules with linear substituents were identified as the first example of MC-dyes to show a cooperative supramolecular polymerization based on dipole-dipole and van der Waals interactions. The UV/Vis spectra for **65** and **66** in chloroform show a blue-shift in the absorption from 589 to 462 nm when the temperature is decreased or the concentration is increased, which is characteristic for an antiparallel arrangement of the MC chromophores with H-type excitonic coupling.
Detailed inspection of the spectral features associated to this self-assembly discloses abrupt changes upon reaching a certain temperature or concentration (Fig. 19a,b). Remarkably, the successful application of the cooperative nucleation-elongation model by van der Schoot to the temperature dependent data as well as the fitting of concentration-dependent studies to the Goldstein-and-Stryer model yields comparable results. The size of the aggregates at the elongation temperature could be defined around 8-10 monomeric units that interact by dipole-dipole forces (Fig. 19c). These one-dimensional stacks further grow into 2D lamellae by the interplay of dipole-dipole interactions between the MCs and lateral van der Waals forces between the alkyl substituents.

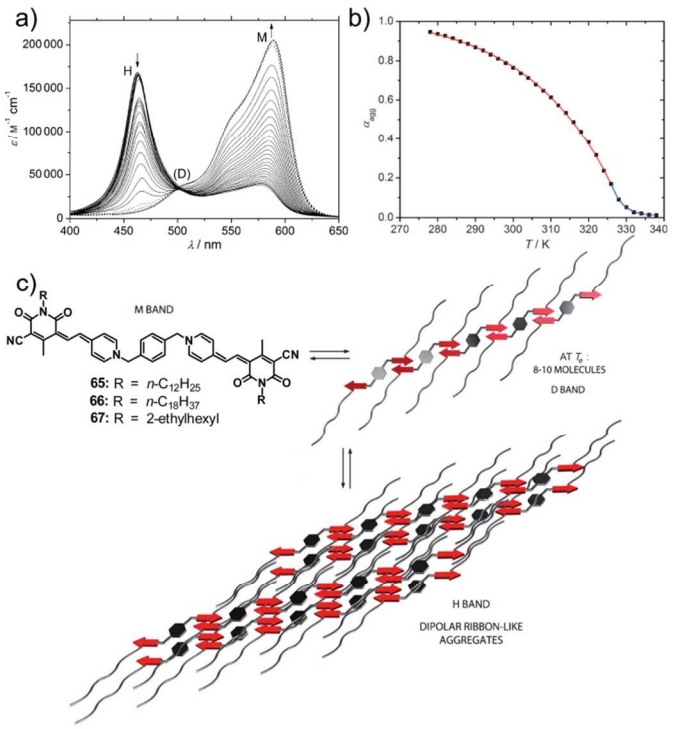

Fig. 19 a) Temperature-dependent UV/Vis spectra of **66** ($CHCl_3$, c = 3.1 x 10^{-6} M), 278 to 338 K. Arrows indicate spectral changes upon increasing temperature. b) Fitting of α_{agg} against *T* in the framework of the nucleation-elongation model by van der Schoot. ~~The blue line corresponds to the nucleation regime and the red line to the elongation regime.~~ Black squares represent the experimental data of **66** obtained in temperature-dependent experiments at λ = 589 nm. c) Proposed self-assembly model for bis(MC) dyes **65** and **66**. Reproduced with permission from refer. 163 (© Wiley VCH).

In a separate work, the same group designed a more sophisticated system based on a Hamilton receptor-tethered bis(MC) **68** that shows a biphasic solvent-induced self-assembly into two distinct species by a sequence of isodesmic and cooperative self-assembly events.[164] The aggregation was thoroughly investigated by means of UV/Vis in THF/MCH mixtures of various ratios (Fig. 20a). In pure THF the monomeric species **A** dominates, while the addition of MCH clearly induces aggregation in two steps (species **B** and **C**) as characterized by two distinguishable isosbestic points.

These two self-assembly processes were also observed in capillary viscosity measurements. Initially, the expected enhancement in the reduced viscosity can be noticed upon increasing concentration, followed by a sudden drop-off above a certain concentration (Fig. 20a, inset), suggesting the appearance of a second species of smaller size.

The UV/Vis spectra at 10^{-5} M from 0 to 70% MCH in THF, corresponding to the first transition, feature an isosbestic point at 517 nm and shows a decrease of the monomer band along with the emergence of a hypsochromically shifted band, indicating the formation of extended H-type aggregates. The data points extracted at a particular wavelength from concentration-dependent UV/Vis studies in MCH/THF = 70:30 (Fig. 20b) perfectly follow a sigmoidal curve that enables a successful fitting to the isodesmic model defining a single binding constant $K \approx 3.9 \times 10^5\ M^{-1}$.

Microscopic imaging reveal long fibers that can further interact into extended networks. The model developed from these findings shows an antiparallel aggregation of the highly dipolar MC moieties resulting in a flexible polymer with the aliphatic units pointing towards the surrounding media (Fig. 20d).

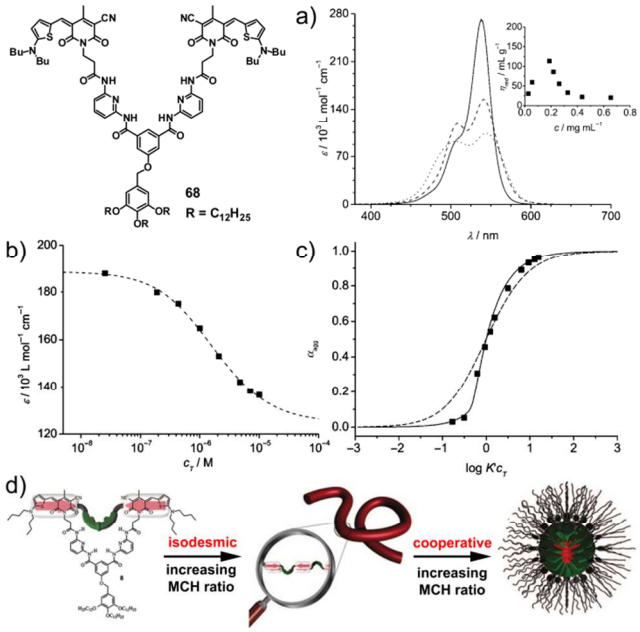

Fig. 20 a) Temperature UV/Vis absorption spectra of monomers **A** (THF/MCH=100:0 vol%, solid line), and self-assembled species **B** (THF/MCH = 40:60 vol%, dashed line) and **C** (THF/MCH=10:90 vol%, dotted line) from **74** (c = 1.0 x 10^{-4} M) at 298 K. The inset shows the reduced viscositiy η_{red} in THF/MCH = 40:60 vol% at different concentrations. b) Apparent absorption coefficient at 533 nm plotted against c_T and the result of the nonlinear regression analysis based on the isodesmic model for the formation of **B**. c) α_{agg} plotted as a function of $\log K' c_T$ according to the isodesmic model (dashed curve) and to the self-assembly of a closed oligomer (solid curve) and plot of the experimental data at 507 nm for the formation of **C** after manual fit of the line shape. d) Schematic representation of the solvent-dependent self-assembly of bis(MC) **68**. Reproduced with permission from refer. 164 (© Wiley VCH).

The second transition at higher MCH content (above 70% at 10^{-5} M) shows an isosbestic point at 496 nm and the spectra broaden resembling a less ordered state. When this transition is monitored by concentration-dependent studies in MCH/THF = 80:20, a distinctly different non-sigmoidal curve is found (Fig. 20c). Characterization by AFM and DLS revealed a spherical morphology with a diameter of ~9.0 nm. The suggested arrangements are inverted micelles and the dipolar MC units are shielded inside the core while the alkyl chains are exposed towards the nonpolar solvent (Fig. 20d). The evidence for globular aggregates initiates the application of a cooperative fitting model that includes the formation of closed systems.[2] Indeed, satisfactory fitting supports the presence of closed species consisting of around 20 molecules that are formed by the cooperative effect of dipolar and hydrogen bonding interactions and further driven by solvophobic effects as the content of apolar solvent increases.

For many years Schmuck and co-workers have exploited the properties of guanidiniocarbonyl pyrrole carboxylate zwitterions in terms of ion binding, receptor ability and self-assembly.[165-172] In 1999, Schmuck and coworkers reported the formation of highly stable dimers of 5-(guanidiniocarbonyl)-1*H*-pyrrole-2-carboxylate

zwitterions in DMSO by multiple weak interactions between the self-complementary binding groups, that was evident from NMR and Molecular modelling.[165] This dimerization was also observed for a similar derivative bearing flexible triethyleneglycol chains at the pyrrol center.[168]
In 2001, the authors designed a related 2-(guanidiniocarbonyl)-pyrrole-4-carboxylate zwitterion that self-assembles into larger (oligomeric) structures in DMSO due to ion pairing between the carboxylate function and the guanidinium group of neighboring monomers resulting in one-dimensional assemblies.[167]

More recently, the authors extended their studies to a series of novel 2-guanidiniocarbonyl pyrrole 5-carboxylate derivatives (**69**-**75**) with different substituents on the pyrrol ring that similarly show an initial dimerization, followed by a further self-association step into different types of arrangements.[173] The molecular structure of the zwitterions is structurally related to the initial molecule studied in 1999,[165] however amide substituents on the central pyrrol facilitate the additional assembly of the dimers into extended aggregates. Microscopic studies of **71** and **72** show extended bundles of laterally interacting fibers with a length of several hundred nanometers and heights that correspond to the formed dimers.
The hierarchical organisation by initial dimerization, followed by π-stacking of the dimerized zwitterions was corroborated by molecular modeling. These calculations show that the dimers, stabilized by self-complementary H-bonding are planar and thus can further grow in one direction driven by aromatic contacts and hydrogen-bonding between the peripheral amide groups. This model also explains why for derivative **70,** lacking the amide proton in the substituent, just as for initial **69**, microscopic imaging did not reveal any discrete structures. UV Studies of **71** in DMSO at various concentrations (10^{-4} to 10^{-9} M) show an isosbestic point at 312 nm, indicative of equilibrium between well-defined structures and a bathochromic shift of the absorption maxima from ~300 to ~320 nm upon decreasing concentration. These spectral changes can be assigned to the organization of the dimers into one-dimensional rods and do not include the dimerization itself since this initial process has already taken place at nanomolar concentration, as indicated by the high dimerization constant ($K > 10^{10}$ M^{-1} in DMSO).[165,168] To examine the mechanism of self-assembly, the degree of aggregation was plotted against the concentration giving rise to a clearly non-sigmoidal curve with a tremendous increase of α upon reaching 10^{-5} M (Fig. 21a).
Fitting to the nucleation-elongation model confirmed a cooperative process with a σ value of 0.09 indicating that the aggregation is split into a nucleation and an elongation event. For the nucleation, two dimers have to come into close contact that requires a planarization of the molecules (Fig. 21b). This goes along with the rotation of the peripheral amide groups out of plane to enable perpendicular hydrogen bonding with neighboring molecules, causing a notable energy penalty. While for the nucleus formation this conformational change has to be accomplished 4 times, every next stacking requires only two rotation events making the initial dimer stacking an unfavorable process while the further stacking can proceed in a cooperative fashion. This orientational change of the amide groups also causes the ~20 nm bathochromic shift in the absorption spectra as shown by DFT calculations.
All other investigated derivatives also followed cooperative self-assembly for the same interactions as mentioned. The peripheral substituents can further be involved in attractive aromatic or van-der-Waals interactions directly affecting the degree of cooperativity and the binding constant, as well as the morphology of the aggregates visualized by microscopic studies.

Due to the sensitivity of the zwitterions to changes in the pH, the protonation of the molecules by addition of HCl leads to a complete structural change, as e.g. for **71** of the extended rod-like arrangements to small vesicles. These self-assemblies of the cationic species **71*H**$^+$ can be transformed back into the initial one-dimensional fibers by a systematic deprotonation to the zwitterionic state.

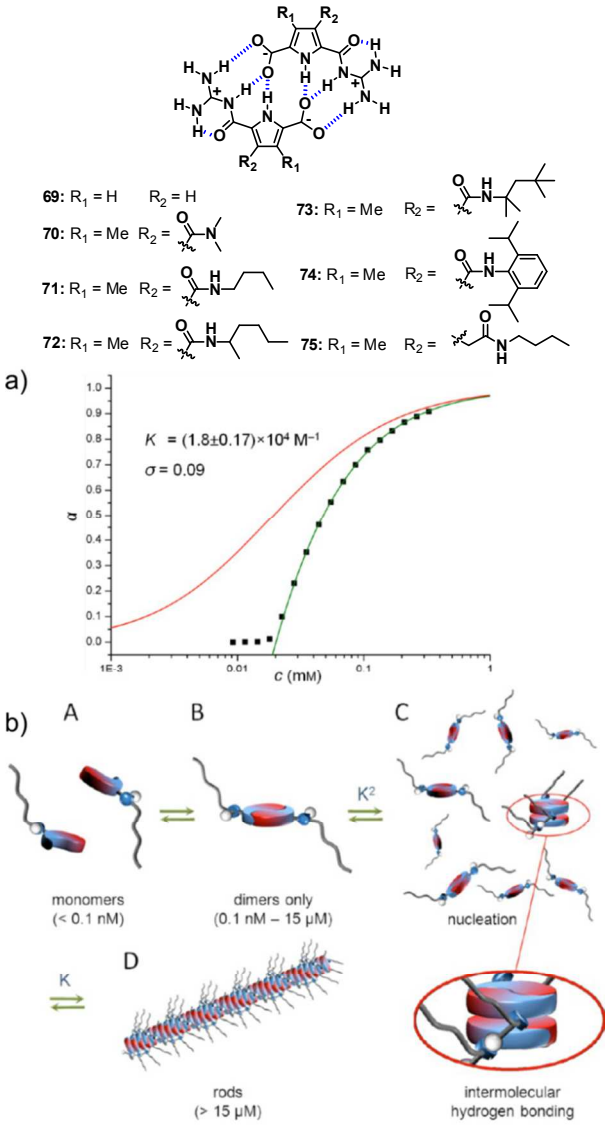

Fig. 21 a) Plot α of **71** against the concentration (black squares). The data can only be fitted to a strongly cooperative aggregation model (green) but clearly not to an isodesmic growth model (red). b) Schematic self-assembly of **71** starting at infinite diluted solution (A) via dimerization (B) and nucleation (C) to formation of one-dimensional rod-like structures (D). Reproduced with permission from refer. 173 (© American Chemical Society).

In 2012, Meijer and co-workers investigated in detail the self-assembly of two series of partially fluorinated BTAs that unexpectedly revealed a two-step aggregation for one series, resulting in the formation of helical assemblies.[174] All investigated molecules contain one fluorinated side chain per molecule, that is decorated with a terminal hydrogen for series **A** (derivatives **76**, **77**) whereas the second series **B** (derivatives **78**-**80**) bears a terminal fluorine atom.

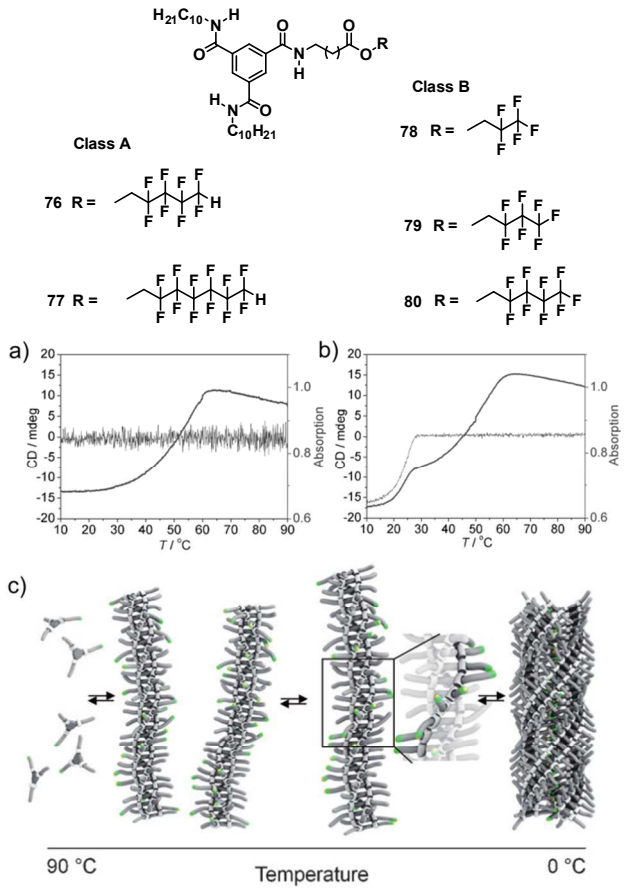

Fig. 22 a,b) Temperature-dependent UV (black) and CD measurements (gray) of a) BTA-F_9 **80** and b) BTA-F_8H **76** (c = 30 mM in MCH, at λ = 223 nm, *l* = 1 cm). c) Proposed self-assembly mechanism for partially fluorinated BTAs of **class A**. Reproduced with permission from refer. 174 (© Wiley VCH).

According to temperature-dependent UV/Vis measurements in MCH, the self-assembly of class **B** (Fig. 22a) occurs in a highly cooperative fashion, mainly driven by hydrogen-bonding interactions that lead to the formation of one-dimensional structures, as already shown for aliphatic-substituted BTAs.[41] Due to the achiral character of the molecules no CD signal appears upon aggregation, clearly indicative of equal ratios of P-type and M-type helices (Fig. 22a).

In contrast, the fiber-like structures formed by achiral class **A** molecules generate a CD effect, as observed in temperature-dependent CD studies below room temperature (Fig. 22b). This unexpected behavior was further investigated by temperature-dependent UV/Vis experiments (Fig. 22b). Cooling down the monomeric state at high temperature, the molecules initially show a comparable behavior to class **B** molecules. Thus, the spectral features can similarly be assigned to the aggregation into P- and M-helical strands lacking any CD effect and following a cooperative aggregation pathway. However, unlike studies of class **B** a second abrupt change at room temperature occurs, that is in agreement with the appearance of the Cotton effect in the CD spectra. This indicates that the self-assembly of class **A** features a further (second) aggregation steps that induces a bundling of the initially formed, optically non-active helices into significantly larger optical-active assemblies, as confirmed by AFM. While the first cooperative step is driven by hydrogen-bonding, the second step must be related to a secondary nucleation with minute amounts of chiral impurities driven by dipole-dipole forces (Fig. 22c).

The suggested model for this two-step mechanism considers that a rearrangement of the molecules in the initially formed helical fibers leads to a fluorine-enriched patch on the fiber surface. This subsequently induces a further bundling of the fibers that is supported by weak attractive interactions between the fluorine atoms of one helix and terminal electron-deficient hydrogen atoms of a neighboring stack. The appearance of a preferred handedness might be attributed to the presence of chiral impurities. The effect of chiral additives was investigated upon adding a small amount of chiral guests to the class **A** solutions in MCH resulting in a significant increase in the CD signals.

3.5 π-π-interactions supported by other weak non-covalent or conformational contributions

The previous examples described in detail that cooperative systems can be the result of cooperative hydrogen bonding interactions or, as most examples show, arise when two or more specific non-covalent interactions act simultaneously. However, a handful of examples of unexpected, slightly cooperative systems can be found in literature that are mainly based on π-π-interactions, supported by important contributions of other weak non-covalent forces or conformational changes.

An illustrative example in this regard was reported by Sanchez and co-workers in 2011.[175] The authors investigated the self-assembly of four triangular-shaped OPEs (**81**-**84**) on surfaces and in solution, three of them featuring chiral aliphatic chains (**81**-**83**) and one literature-known[176,177] achiral OPE bearing a non-branched alkyl substituent (**84**).

AFM images of the two enantiomers (*S*)-**81** and (*R*)-**82** in MCH exhibiting a stereogenic center in the 3-position of the alkyl substituent displayed rope-like aggregates with lengths of several micrometers and a height that corresponds to a single-molecule length (Fig. 23a,b). These structures exhibit opposed handedness originated from the opposite chirality in the molecular design. These left- and right-handed structures for (*S*)-**81** and (*R*)-**82**, respectively are formed by π-π-stacking interactions between the aromatic cores with an opposite mutual rotation of the discs. Similarly, helical stacks were also created by the chiral derivative (*S*)-**83**. However, these right-handed helices unexpectedly exhibit an opposite handedness to the assemblies formed by *(S)*-**81** with the same stereoconfiguration. Furthermore, the helical pitch for the (*S*)-**83** helix is smaller than that for the (*S*)-**81** aggregates indicating that the position of the chiral methyl group and the (branched) nature of the aliphatic substituents have a significant influence on the direction and magnitude of rotation of the subunits within the stack. The aggregation of achiral **84** also results in helical arrangements, even though the amounts of P- and M-type columnar assemblies are equal.

The self-assembly behavior of (*S*)-**83** in MCH was investigated by concentration-dependent UV/Vis experiments showing significant changes upon increasing concentration owing to π-stacking interactions. Plotting α_{agg} against the concentration gives rise to a sigmoidal curve, revealing that (*S*)-**83** self-assembles in an isodesmic fashion. Similar results were obtained for the self-assembly of achiral **84**.[177] In contrast, fitting of the concentration-dependent α_{agg} values to the isodemic model failed for the chiral counterparts (*S*)-**81** and (*R*)-**82**, clearly indicating that the monomer-to-aggregate transition follows a cooperative pathway.[175]

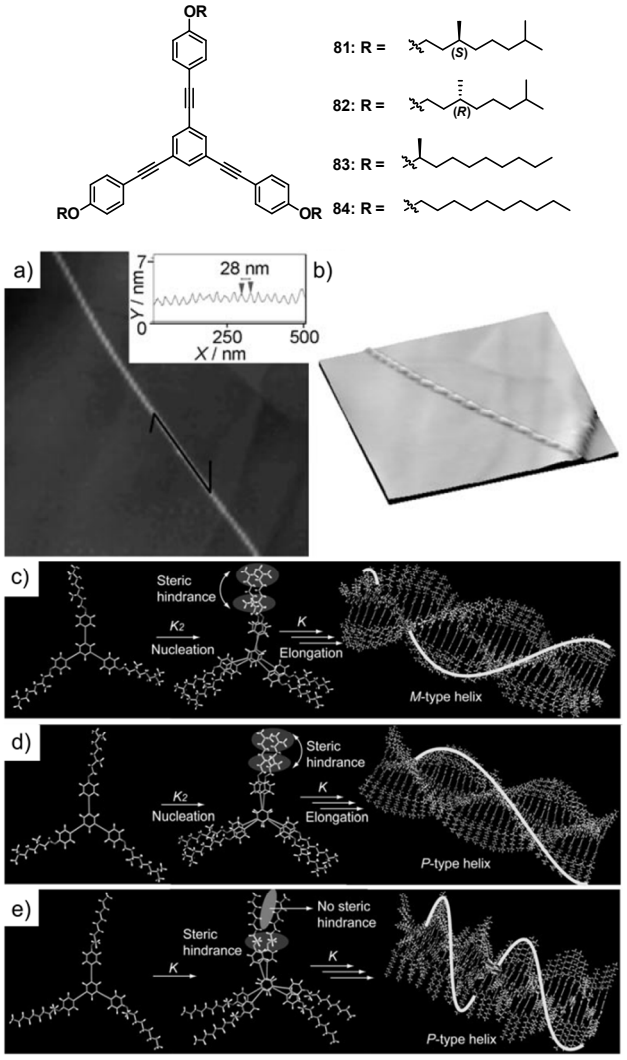

Fig. 23 a,b) Tapping-mode AFM images (air, 298 K) of a spin-cast MCH solution (~10^{-4} M, HOPG) of a) (*S*)-**81** showing a M-type helix (Z scale=10 nm), and b) (*R*)-**82** showing a P-type helix (Z scale=10 nm). The insets depict the corresponding height profile and the helical pitch along the black line. c-e) Schematic illustration of the self-assembly of c) (*S*)-**81**, d) (*R*)-**82** and e) (*S*)-**83**. The line depicts the helicity of the aggregates. Reproduced with permission from refer. 175 (© Wiley VCH).

Application of the cooperative K_2-K nucleation-elongation model [36,45] yielded satisfactory fits for a cooperativity factor $\sigma = 0.2$ giving comparable thermodynamic parameters for the aggregation of (*S*)-**81** and (*R*)-**82**. Although, the degree of cooperativity (with a σ value of 0.2) is relatively low, it is somewhat unexpected in these systems because the aggregation affinity is mainly based on π-π-interactions. Comparing the molecular design of (*S*)-**81** and (*R*)-**82** with (*S*)-**83**, the only structural variation, most likely responsible for the slight cooperativity in the aggregation process, lies in the position of the stereogenic center and the branched nature of the peripheral substituent in (*S*)-**81** and (*R*)-**82** (Fig. 23c-e). Thus, when initially two monomeric molecules come in close contact by π-π-interactions, conformational changes are necessary to reduce the steric demand of the bulky substituents. This process represents the unfavorable step, characterized by a relatively low binding constant of 2.6 x 10^4 M^{-1} and can thus be regarded as the nucleation event. The association of a third or fourth molecule requires less pronounced conformational changes resulting in a twenty-fold higher binding constant and thus defined as the elongation step.

Recently, Würthner and co-workers reported two pieces of work regarding the self-assembly of perylene bisimide (PBI) dyads (**85**, **86**) showing that a variation in the backbone length induces a change in the self-assembly from dimerization to cooperative elongated π-stacks.[80,178] In their initial work they synthesized dyad **85**, constructed of two PBI chromophores both capped with branched alkyl chains and connected by a diphenylacetylene (DPA) unit as backbone.[178] This molecule aggregates into stable interlocked dimers due to the perfect matching of the PBI distance to stable π-π-interactions. In the following studies the structural motif was maintained but the connecting unit elongated to a diphenylbutadiyne (DPB) spacer (derivative **86**) leading to a PBI-PBI distance that is three times the expected distance for aromatic PBI stacking.[80]

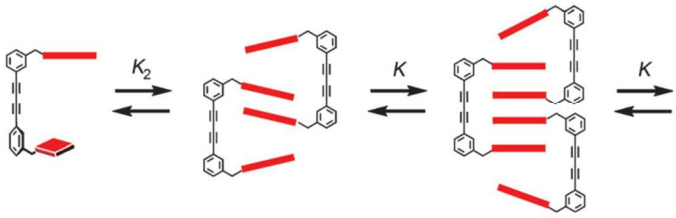

Fig. 24 Model of the backbone-directed "arm-in-arm" aggregation of PBI **86** into extended oligomeric π-stacks. Reproduced with permission from refer. 80 (© Wiley VCH).

MALDI-TOF spectra of a MCH solution revealed the presence of extended aggregates of up to 21 dyads of **86** that could be confirmed by DOSY measurements. Concentration-dependent UV/Vis studies in Chloroform/MCH = 30:70 monitored the transition from aggregated to monomeric species with the plot of α_{agg} against Kc_T being non-sigmoidal. At first glance, this behavior is rather unexpected since π-π-interactions constitute the sole intermolecular force between the PBI surfaces. This single attraction thus results in a value of $\sigma = 0.1$ for the fitting to the cooperative K_2-K model, revealing that the aggregation pathway for **86** is slightly cooperative. This behavior is contrary to the PBI precursor **87**, representing only half of the investigated dyad that aggregates in a non-cooperative fashion into much less stable aggregates. The cooperative character of **86** was further confirmed by kinetic studies regarding the time-dependent deaggregation upon dilution of a highly aggregated sample. The spectral changes upon disassembly exhibit several isosbestic points that reveal the existence of only two defined states (monomeric and aggregated). Furthermore, the changes over time follow a first order kinetics, also indicating that the oligomers of **86** disassemble cooperatively.

These results indicate that the dyad assembly is divided into an unfavorable dimerization that is followed by an elongation step characterized by a tenfold higher binding constant. Due to the presence of only π-π-interactions as interactive forces, the second important driving force contributing to the cooperative mechanism can be explained by considering the arrangement of the chromophores in the stack. As already mentioned, the molecular design of **86** includes a PBI distance that is three times the ideal value for perfect π-π-interactions (3.3-3.4 Å), thus enabling an "arm-in-arm" aggregation (Fig. 24). Regarding the nucleation step, only one PBI surface enters this space, resulting in a comparatively weak π-interaction. However, in the elongation process these dimers can interdigitate to perfectly fill this intramolecular space, resulting in a more stable association of dense elongated π-stacks. However, similar to the previous example of triangular-shaped OPEs from Sanchez and co-workers,[175] this example points out again that π-π-interactions as single attractive interaction can, if at all, only result in a weak cooperative strength.

In 2007, the groups of De Feyter, Meijer and Schenning studied the self-assembly of an oligo(*p*-phenylenevinylene) (OPV)-substituted hexaarylbenzene by various techniques in solution and on surface.[179] Star-shaped molecule **88** features a hexaarylbenzene center that is connected to six OPV segments decorated with branched chiral (*S*)-side chains resulting in a propeller-like structure.

Thermogravimetric analysis (TGA) of **88** shows that this molecule is stable up to 300°C and upon slow cooling from the molten sample a crystalline phase can be visualized by means of polarized optical microscopy (POM) revealing a fan-shaped texture (Fig. 25a). This high degree of order in the plastic crystalline phase can also be detected in 2D WAXS studies that revealed perfect columnar stacking of the molecules whose OPV-propeller arms are not completely planar but slightly rotated. UV/Vis measurements indicated that OPV **88** exists in an aggregated state in heptane solution that could be further characterized by CD as helical stacks. These arrangements showed to be stable up to 90°C, also for a highly diluted sample of 10^{-7} M. In contrast, switching to MCH allowed the disassembly of the helical species upon heating from room to high temperature. The cooling curves associated to this transition, according to both UV/Vis and CD measurements, are clearly non-sigmoidal with a significant onset of aggregation at the elongation temperature T_e = 331 K (Fig. 25b). Fitting the UV data to the nucleation-growth model[40,41] determined an average size of the assemblies at T_e of around 32 molecules that grow into π-stacked arrangements of more than 10000 subunits at room temperature, as confirmed by AFM.

A close-up shot of an aggregate sample revealed the formation of chiral arrangements that consist of around 18 molecules per turn, as illustrated in Fig. 25c. This confirms a dense packing of the OPV units by efficient π-π-stacking provided by the pronounced overlap of the aromatic surfaces of the slightly rotated propeller arms. As the detailed investigation shows, the arrangement into chiral stacks follows a highly cooperative mechanism with a remarkably low K_a value of 3 x 10^{-5} although π-π-interactions represent the chief attractive forces in the system. ~~This is rather special because in general, a cooperative growth takes place when at least a second important contribution comes into play.~~

One possible explanation can be seen in the conformational changes that are necessary to start the effective interaction with adjacent subunits. While in non-aggregating solution the propeller arms of the OPVs are independent and can freely rotate, the activation of the monomer affords conformational changes. To enable effective π-interactions, the six arms of the molecule have to adopt a more ordered conformation that is accomplished in an unfavourable rearrangement of the molecular scaffold. ~~resulting in formation of the unfavourable nucleus.~~ Once this is overcome, the system can elongate by favourable association of further molecules into extended helical structures.

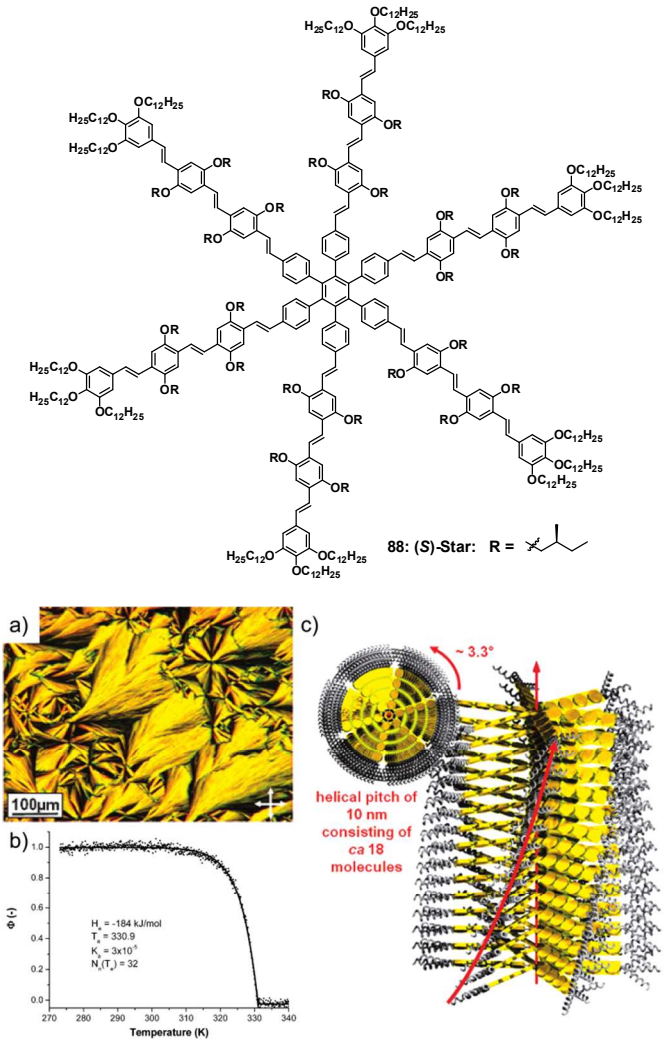

Fig. 25 a) Image from polarized optical microscopy of the star-shaped OPV **88** b) Fit of the normalized melting curve using the nucleation-growth model. c) Schematic illustration of the helical columnar packing based on X-ray, CD and AFM data. Reproduced with permission from refer. 179 (© American Chemical Society).

Although this explanation is similar to that of the triangular-shaped OPEs reported by Sanchez and coworkers,[175] the cooperative strength of star-shaped OPV **88**[179] is much more pronounced than in this system and also than that exhibited by the PBI dyad **86** of Würthner and coworkers[159]. The reason for this might be related to flexibility and conformation aspects of the chromophores. The presence of a sterically crowded hexasubstituted central benzene ring in **88** induces a conformational adaption of the propeller arms out of plane that can occur unrestrictedly around the single bond in the OPV system, unlike more rigid OPEs **81-82** and and PBI **86** in which this motion is restricted. Furthermore, in comparison to the presented OPEs[175] and the PBI[80], the extended OPV arms are much more flexible, which might facilitate conformational changes and closer packing of the subunits that are essential for the stable growth of the system.

3.6 Cooperative Systems in water

Due to the unique properties of water, the self-assembly in this media is highly influenced by the well-known "hydrophobic effect".[180-184] The origin of this unique effect lies in the fact that the interactions of water molecules among each other are much more favorable than the interactions of water molecules with non-polar groups (hydrophobic surfaces). Solvation of a non-polar solute leads to a cleavage of hydrogen bonding interactions when its size is not fitting within the cavities of the water network. To minimize this loss of highly attractive interactions, the added molecules are forced to aggregate into larger clusters, thus the hydrogen-bonding network can be maintained to the greatest possible extent. This generates a strong driving force for self-assembly of amphiphilic molecules in aqueous media[10,75,121,185-194] compared to an organic solvent environment that can additionally contribute to induce cooperative phenomena.
In the following, we have collected and classified the most remarkable examples of cooperative supramolecular polymers in water that are driven, besides the hydrophobic effect, by other non-covalent interactions.

3.6.1 Encapsulation / Co-Assembly

In 2012, our working group showed an intriguing example of a water-soluble linear oligophenylene(ethynylene) (OPE) amphiphile **89** whose aggregate morphology and self(co)-assembly mechanism (isodesmic or cooperative) can be controlled by the addition of a related hydrophobic OPE **90** with similar shape.[195] Furthermore, the self-assembly of an equimolar mixture into independent (narcissistic) or co-assembled (social) aggregates was observed to strongly depend on the investigated concentration.
The molecules consist of three linear OPE units equipped with three triethyleneglycol (**89**) and alkyl chains (**90**) on each side, respectively. The water-soluble derivative **89** shows a propensity to aggregate in water by aromatic interactions, as evidenced by a significant emission quenching upon increasing concentration.
The spectral changes during variable-temperature UV/Vis studies are characterized by a defined isosbestic point indicating equilibrium between well-defined species. Switching to the less polar solvent mixture THF/water = 1:1 showed a similar self-assembly behavior. The cooling curves at certain wavelength showed a sigmoidal shape for both samples (THF and THF/water), indicative of an isodesmic process and confirmed by good fitting to the non-cooperative model. AFM and SEM images as well as DLS studies of the arrangements of **89** in both media revealed spherical objects of 3–10 nm size driven by π-π-stacking between the OPE cores with the triethyleneglycol chains exposed towards the solvent acting as hydrophilic micelle shell.
On the other hand, non-amphiphilic derivative **90** shows a strong aggregation tendency in THF (10^{-5} M) when 30% water is added, while at mM concentration the compound directly precipitates due to its remarkable hydrophobicity. Microscopic and DLS studies of **90** revealed similar results as for the amphiphilic counterpart **89** showing discrete spherical assemblies that further conglomerate due to the hydrophobic effect giving rise to particles of up to 50 nm.
The self-sorting behavior upon mixing these two aggregating species showed a pronounced concentration-dependence. In THF/water = 1:1 at 10^{-5} M, a clear narcissistic self-sorting occurs, as evidenced by the UV/Vis spectra representing an overlay of the absorption of the two distinct compounds and by the appearance of only spherical aggregates in SEM studies (Fig. 26a and 26c top). However, when the concentration is increased to 1 mM, a clear co-assembly process can be observed, driven by the hydrophobic effect and facilitated by the identical size of the aromatic OPE cores. This social self-sorting behavior results in the appearance of a red-shifted transition (400–500nm) in the UV/Vis spectra upon addition of water to a 1:1 mixture of **89** and **90,** that was absent at lower concentration.

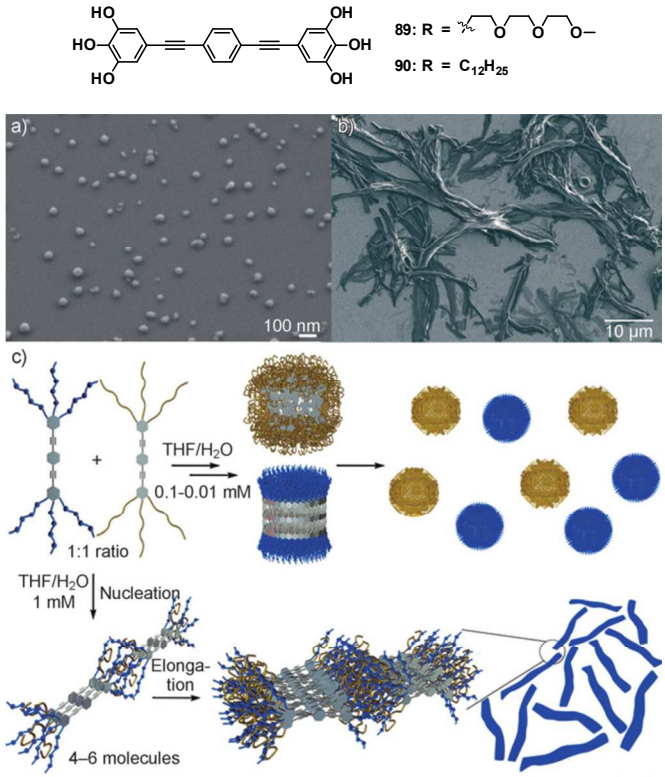

Fig. 26 SEM images obtained by spin-coating a 1:1 mixture of **89** and **90** in THF/water at a) c = 0.1 mM and b) c = 1 mM on a silicon wafer. c) Cartoon representation of the concentration-dependent self-sorting behavior of a 1:1 mixture of **89** and **90** in THF/water (1:1). Narcissistic self-sorting between c = 0.01 and c = 0.1 mM (top) and social self-sorting at c = 1 mM (bottom). Reproduced with permission from refer. 195 (© Wiley VCH).

Analysis of temperature-dependent UV/Vis studies of a 1:1 mixture in THF/water (6:4) reveal a cooperative aggregation pathway that can be described by the nucleation–elongation model developed by Schenning, Meijer and van der Schoot[40,41] determining an aggregate size at T_e of 6 molecules. This co-assembly process is accompanied by notable structural changes, as could be visualized by SEM. While the isodesmic self-assembly of the individual compound gave rise to spherical particles, the co-assembly results in the cooperative formation of extended ribbons with a length of up to several micrometers (Fig. 26b and 26c bottom).

Recently, our group extended the studies on co-assembly processes in aqueous media and investigated the self-assembly of an OPE-4,4-difluoro-4-bora-3a,4a-diaza-*s*-indacene (BODIPY) bola-amphiphile **91** in water and its size-dependent co-assembly phenomena with small aromatic molecules, such as tetracene and anthracene.[196] UV/Vis and fluorescence experiments suggest that **91** self-assembles in water into H-type aggregates that are stabilized by π-π-interactions, characterized by a twisted conformation of the subunits in the assemblies. Temperature-dependent investigation showed a reversible transition between the monomeric and aggregated state that is defined by a sigmoidal cooling curve. Applying the isodesmic

model confirmed the non-cooperative pathway with binding constants around 1 x 10^6 M^{-1}.

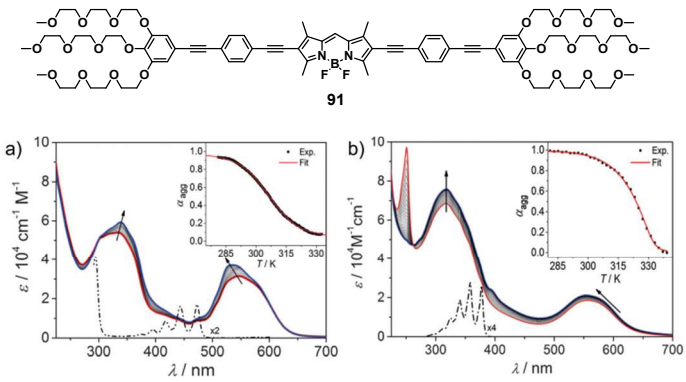

Fig. 27 Temperature-dependent UV/Vis studies of **91** in aqueous solution (10^{-5} M) containing one equivalent of a) tetracene and b) anthracene. Arrows indicate spectral changes upon temperature decrease. Dash-dotted line: UV/Vis spectra of a) tetracene and b) anthracene in THF. Inset in a): Fitting of α_{agg} at 510 nm to the isodesmic model. Inset in b) Fitting of α_{agg} at 555 nm to the ten Eikelder–Markvoort–Meijer model. Reproduced with permission from refer. 196 (© Wiley VCH).

The hydrophobic interior of the fibrils that is shielded from the aqueous media by the hydrophilic glycol shell was further tested for the embedding of hydrophobic guest chromophores, such as tetracene and anthracene. Both molecules are insoluble in water and precipitate out rapidly, facilitating the detection of encapsulation by the naked eye. Indeed, the addition of either 1 eq of tetracene or anthracene to an aggregate solution of BODIPY **91** in water results in a clear solution, indicating the successful uptake of the insoluble dye molecules within the assemblies. This co-assembly can also be detected in the UV/Vis spectra, exhibiting a new, albeit weak absorption maximum corresponding to the dyes. Although Job's plot analysis reveals an identical host:guest binding stoichiometry for both dyes of 1:1, their co-assembly occurs in a distinct fashion, as shown by temperature-dependent encapsulation studies (Fig. 27).

By monitoring the cooling curve of the mixture with tetracene (Fig. 27a, inset), a sigmoidal curve is obtained, indicating that the co-assembly proceeds in an isodesmic manner. This non-cooperative co-aggregation induces a stiffening and elongation of the fibers, while the internal order is not increased (Fig. 28, top). In contrast, the cooling curve associated to the co-assembly with the smaller dye anthracene (Fig. 27b, inset) can be clearly described as cooperative process, accompanied by a change in the morphology of the aggregates to highly-ordered spherical micelles (Fig. 28, bottom).

These results indicate not only that slight structural changes in the guest molecule induce a fascinating switch in the aggregation pathway, but also that hydrophobic interactions can become strong enough to induce cooperative effects.

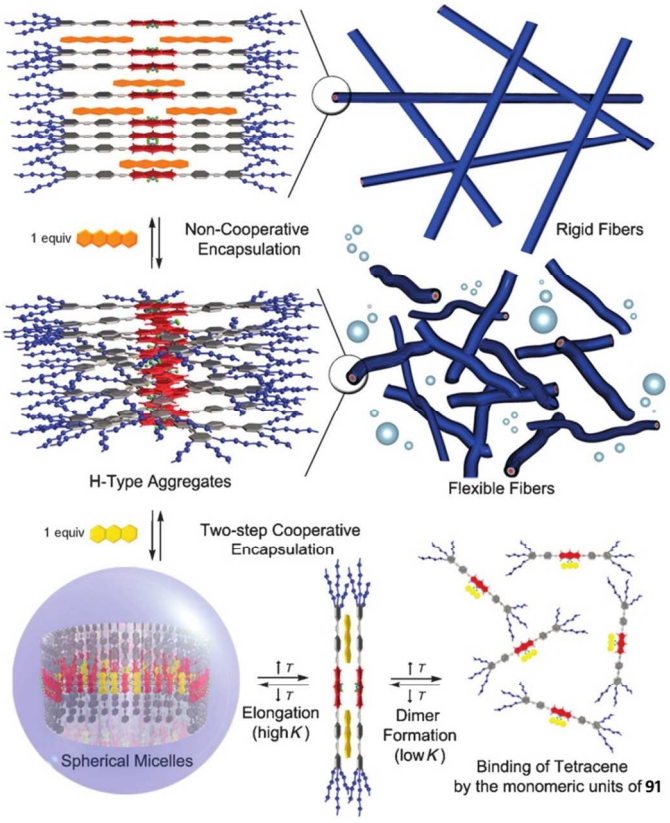

Fig. 28 Cartoon representation of the self-assembly of **91** into H-type aggregates and its reversible guest-dependent encapsulation processes. Reproduced with permission from refer. 196 (© Wiley VCH).

3.6.2 π-π-, the hydrophobic effect (and hydrogen bonding interactions)

Very recently, Rybtchinski and co-workers have investigated two unsymmetrically bay-substituted PBI amphiphiles with a solubilizing glycol group on one side and an aniline amide on the opposite side bearing either a linear alkyl chain (**92**) or a perfluorinated end group (**93**).[197] Comparing these structurally similar derivatives, the authors delivered insight into the influence of the highly hydrophobic fluorocarbon group on the self-assembly behavior.

Regarding the absorption studies in THF/water mixtures of varying ratio, both compounds **92** and **93** show similar spectral changes upon increasing water content that were characteristic for an H-type stacking with a slight rotation of the subunits. Cryo-TEM studies in water/THF (65:35) showed fiber-like structures for both derivatives (Fig. 29 a), with smaller assemblies formed by **92**. The dimensions match well with linearly π-stacked PBIs that fill the inner fiber compartment surrounded, in the case of **93**, by the (fluoro)alkyl substituents exposed towards surrounding media. Due to the more flexible character of the H-chains in **92** they are in close contact with the inner PBI units while the F-chains in **93** are rigid and have an extended conformation resulting in a larger diameter for the F-derivative (Fig. 29a). These assemblies are most likely further supported by hydrogen bonding interactions that are possible even in aqueous media due to the hydrophobic environment of the hydrogen bonding units in the molecular structure.

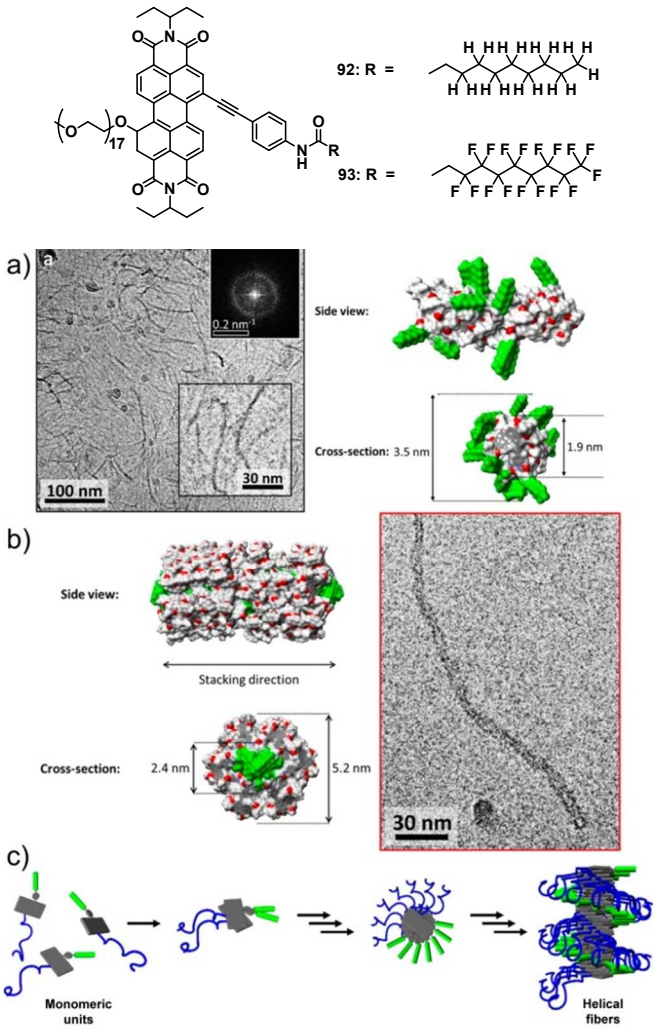

Fig 29. a, left) Cryo- TEM image of **93** (10^{-4} M) in 65:35 water/THF (v/v). Inset: FFT of the image, revealing a periodicity of ~8.2 nm, which corresponds to the average fiber–fiber spacing. (a, right) Proposed molecular model of the supramolecular fibers of **93**. b, right) High-magnification cryo-TEM images of tube-like fibers of **93** (10^{-4} M) in 70:30 water/THF (v/v). b, left) Proposed molecular model. c) Schematic illustration of the proposed mechanism of the cooperative aggregation of **93**. Reproduced with permission from refer. 197 (© American Chemical Society).

Upon increasing the water content to 80%, the assemblies of **92** are barely influenced while assemblies of **93** undergo a morphological transformation (Fig. 29b). Still, fiber-like structures are present but of larger diameter (5-6 nm). Closer inspection of cryo-TEM images indicated that the perfluorooctyl chains are embedded in the fiber core due to increased hydrophobic interactions while the outer layer consists of densely π-stacked PBI chromophores (Fig. 29b).
Temperature-dependent UV/vis studies show that the structural reorganization of **93** observed in cryo-TEM upon increasing water content is accompanied by unexpected spectral changes. The measurements for a water content of 65 % show monomeric species at 65 °C that self-assemble upon decreasing temperature, characterized by the appearance of a defined isosbestic point. The cooling curves feature a steep slope, indicative of a nucleation-elongation mechanism that was perfectly described by the cooperative model.[37,39-41] In contrast, the aggregation into reversed fibers at higher water content clearly follows an isodesmic pathway. This difference indicates that the water content directly dictates the molecular organization within the stacks and in this regard the corresponding aggregation mechanism. Those changes do not occur for the derivative **92**, characterized by an isodesmic aggregation mechanism independent of the water content. The cooperative formation of the thinner fibers of **93** can be rationalized by considering the helical arrangement of the molecules and the remarkable hydrophobicity of the rigid F-chains. As described in Fig. 29c, in this molecular organization the bulky F-chains, just as the triethyleneglycol groups, point towards the aqueous solvent. The contact of the F-chains with this environment is clearly unfavorable. However, the unattractive contact surface can be reduced once the stacks reach a certain length and the F-chains can be surrounded by the flexible hydrophilic PEG chains of interacting subunits, resulting in a shielding from the polar media. In the first association steps, this stabilization is not yet possible since the chains are oriented at opposite sides of the stack. However once the stack finishes a half-helical turn each further associated molecule contributes to the stabilization of the system, thus turning these steps into a favorable elongation of the system. This helicity explanation also includes the non-cooperativity of the tube-like structures of **93** formed at higher water content due to the lack of helicity in these one-dimensional structures.

Very recently, our group has demonstated that the interplay of π-π- and multiple unconventional C-H···X hydrogen bonding interactions can trigger the cooperative self-assembly and (hydro)gelation of an amphiphilic Pt(II) complex **95** (Chart 4).[198] Water-soluble ligand **94** consists of a linear OPE-core, substituted on one side with a pyridyl ring as metal coordinating moiety and appended to three peripheral triethyleneglycol chains on the opposite edge.

Chart 4 Molecular structures of Compounds **94** and **95**

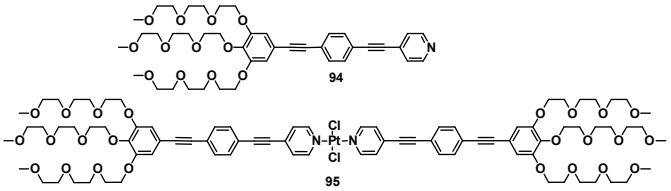

Temperature-dependent measurements nicely show that **94** aggregates in water in an isodesmic fashion into short worm-like structures that can further interact by their flexible glycol chains resulting in a network-like arrangement. The isodesmic self-assembly of ligand **94** can be rationalized since π-stacking between the OPE surfaces represent the single attraction between the molecules. Remarkably, coordination of the ligand to the Pt(II) center affords an amphiphilic square-planar complex **95** whose aggregated state in alcoholic and aqueous solutions exhibit an intense yellow color in contrast to the colorless monomeric state. Upon further increasing the concentration, the gelation of different alcohols and water could be observed. Temperature-dependent UV/Vis studies in MeOH/water (70:30) showed the depletion of the monomer band while a new red-shifted band at 370 nm appeared upon cooling a solution from its monomeric to the self-assembled state (Fig. 30a). The plot of α_{agg} at 420nm against temperature clearly shows for all investigated concentrations a non-sigmoidal shape corresponding to a non-isodesmic process (Fig. 30b). Indeed, the fitting to the cooperative nucleation-elongation model[42,43] gave rise to dimerization constants from 7 M^{-1} to 64 M^{-1} while the association constant for the favorable elongation step lies in the

range of 4300 to 8000 M^{-1}, clearly revealing a highly cooperative process (σ value from 1 to $10x10^{-3}$).

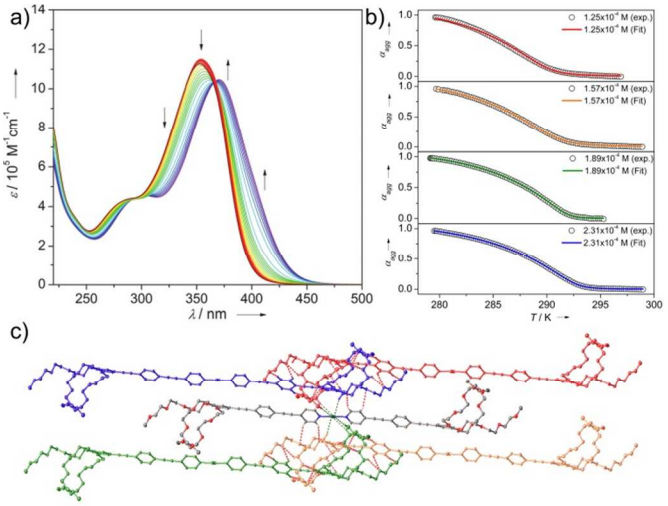

Fig. 30 a) Temperature-dependent UV/Vis experiments of **95** ($MeOH/H_2O$ (70:30), c = 1.28 x 10^{-4} M). Arrows indicate the spectral changes upon decreasing temperature. b) Plot of α_{agg} at 420 nm at four different concentrations ($MeOH/H_2O$ (70:30)). Colored lines represent the fits to the ten Eikelder-Markvoort-Meijer cooperative model. c) Packing of **95** driven by C-H···Cl (green) and C-H···O (red) hydrogen-bonding interactions. Reproduced with permission from refer. 198 (© Wiley VCH).

The 2D NMR studies (ROESY) in methanol revealed a slipped arrangement of the molecules most likely stabilized by attractive π-π- and Cl···π interactions, which perfectly matches the molecular packing observed in the crystal structure from methanol solution. The crystal structure reveals the formation of translationally slipped stacks driven by CH-π interactions, supported by multiple cooperative C-H···Cl and C-H···O hydrogen bondings (Fig. 30c). The presence of sterically demanding Cl ligands attached to the Pt(II) center along with bulky TEG chains prevents a parallel arrangement of the monomeric units of **95** and thus additional metal-metal contacts. As a result, the system rearranges to minimize the repulsive forces. This can be achieved by interactions of the chlorine ligands of the Cl-Pt(II)-Cl center with the glycol chains of four different molecules, which enables the growth of the system in a preferred direction. Simultaneously, we unexpectedly discovered a new class of supramolecular motif that resulted to be the chief driving force for the packing in the crystal state: the TEG chains of each molecule act as glue to the TEG chains of two adjoining molecules driven by multiple C-H···O hydrogen bonds, creating what we termed a "*handshake-like*" structure, as shown in Fig. 30c. The inference from all studies confirmed the interplay between various classes of weak forces (Cl···π, C-H···π, C-H···Cl and C-H···O) as driving force for the cooperative formation of supramolecular polymers and gels by **95**.

Recently, we have exploited this handshake-motif to create cooperative systems, based on related Pd(II) amphiphilic complexes.[199]

3.6.3 Ionic/electrostatic interactions and the hydrophobic effect

Meijer and co-workers studied in detail the fine balance between attractive and repulsive interactions in supramolecular systems and their influence on the morphology and aggregation mechanism of the self-assembled structures.[200] Furthermore they could show that the ionic strength of the aqueous environment can dramatically influence the aggregation process.
They synthesized three discotic BTA derivatives (**96-98**) all sharing a fluorinated phenylalanine substituent and an aminobenzoate function as connecting unit to a hydrophilic metal complex.

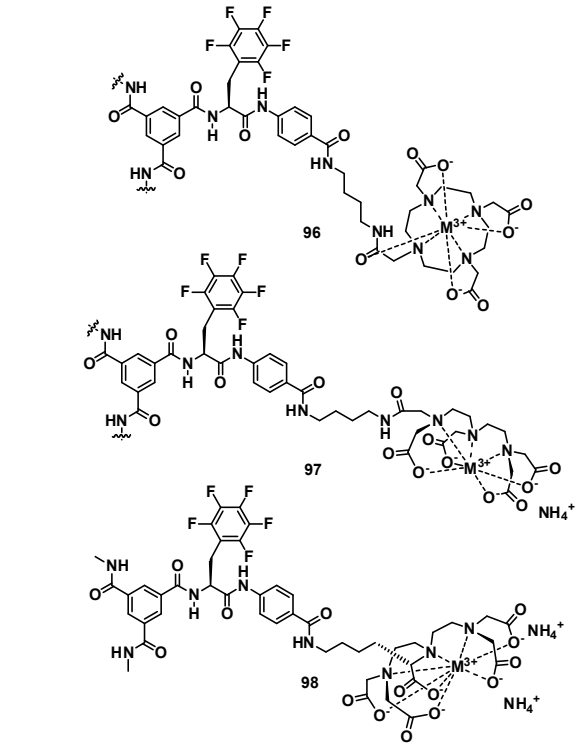

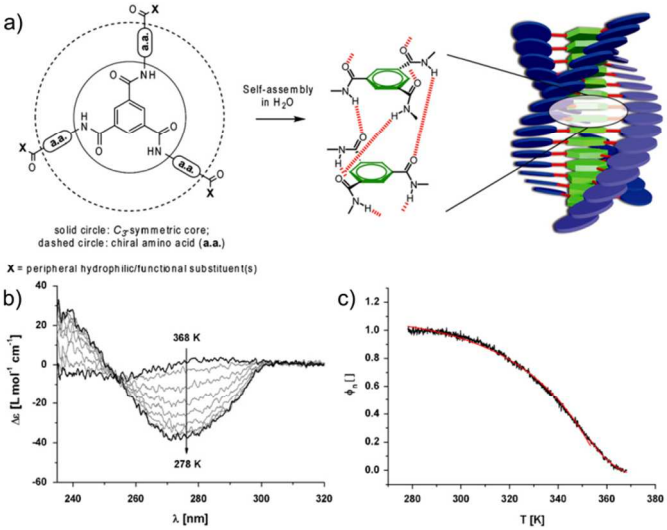

Fig. 31 a) Schematic representation of the self-assembly of discotic amphiphiles. b) Temperature-dependent CD spectra in a c = 100 mM citrate buffer at pH 6 of discotic **96** (c = 5 x 10^{-6} M) and the resulting normalized and fitted CD cooling curves as degree of aggregation Φ_n vs. temperature monitored at λ = 282 nm. Reproduced with permission from refer. 200 (© Proceedings of the National Academy of Sciences of the US).

The molecular design of **96-98** enables a self-assembly of the molecules by hydrogen-bonding and π-π-interactions (Fig. 31a). The three derivatives differ in the nature of the metal complex varying

from charge-neutral (**96**) to negative complexes with one (**97**) or two (**98**) charges per terminal unit.
The dissimilar nature of the systems in terms of repulsive electrostatic forces induce significant changes in the aggregate morphology of **96-98**, as suggested by Small Angle X-Ray Scattering (SAXS) and cryo-TEM studies. For **96** in citrate buffer, rod-like structures of single-molecule diameter could be observed whose lengths depends on the concentration of the sample. In contrast, the six-fold negative-charged BTA **98** self-assembles into spherical objects of around 5nm size at 1mM. Not only do repulsive Columbic interactions control the morphology of the helical aggregates, but also the mechanism of self-assembly under buffered conditions. Cooling curves extracted from temperature-dependent CD (Fig. 31 b,c) and UV/Vis studies show that both neutral BTA **96** as well as singly-charged complex **97** self-assemble in a cooperative fashion. The application of a nucleation-elongation model[37,39] to the non-sigmoidal curve gives the thermodynamic parameters with the activation constant K_a of 10^{-4} for **96** and 10^{-3} for **97** and elongation-temperatures T_e that increase with increasing concentration. However, the organisation of **98** into spherical structures is characterized by a sigmoidal curve indicating that this derivative aggregates in an isodesmic or even anticooperative fashion.[20] Combining these results, the authors concluded that the cooperative supramolecular polymerization no longer exists when the repulsive ionic character of the molecules dramatically increases resulting in the formation of discrete objects with reduced degree of polymerization.
However, one has to note that the self-assembly process for **98** can also be controlled by changing the buffered environment. Upon increasing the ionic strength of the aqueous solution, instead of taking the citrate buffer, the non-cooperative aggregation of **98** can be turned into a cooperative growth. This cooperative process results in the formation of extended rod-like structures, similarly to the assemblies formed by the less-charged BTA derivatives in citrate buffer.

Later on, the same group synthesized three further amphiphilic BTAs **99**-**101**, similarly decorated with a peripheral Gd^{III}-DTPA complex that is attached to the hydrophobic BTA core by different linker units (Chart 5).[201]

Chart 5 Molecular structures of compounds **99**-**101**

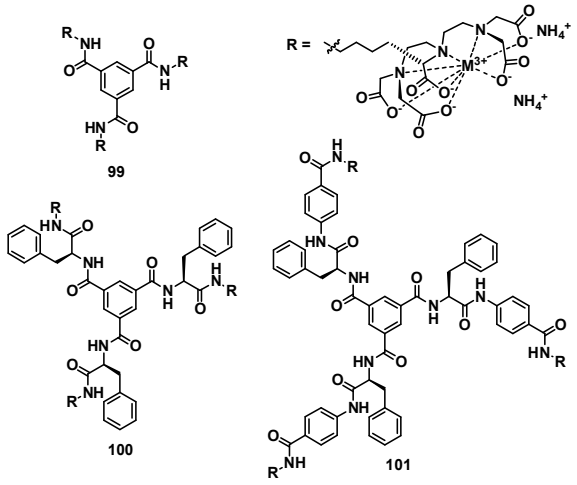

Extensive studies show that the length of this hydrophobic spacer units directly dictates the self-assembly of the molecules. For the smallest discotic **99**, no self-assembled structures could be observed over the whole investigated concentration range indicating that the molecule exists in its monomeric state. Upon elongation of the hydrophobic spacer, the aggregation ability of **100** shows a clear concentration-dependence while the largest discotics **101** directly aggregate into helical stacks in a non- or anti-cooperative manner. These significant differences between the derivatives indicate that the ability to form stable aggregates clearly depends on the length of the hydrophobic spacer. Once the spacers reaches a certain length, it enables an efficient hydrophobic shielding of the triple hydrogen-bonding amide functions of the BTA core through solvophobic effects that results in the formation of stable, helical aggregates.

Very recently, Besenius and co-workers studied the individual self-assembly and co-assembly of two complementary supramolecular monomers in water (**102** and **103**).[202] They consist of a C_3-symmetrical core bearing pentapeptide sidearms decorated with either positively or negatively charged groups that are complementary to each other by hydrogen bonding interactions.

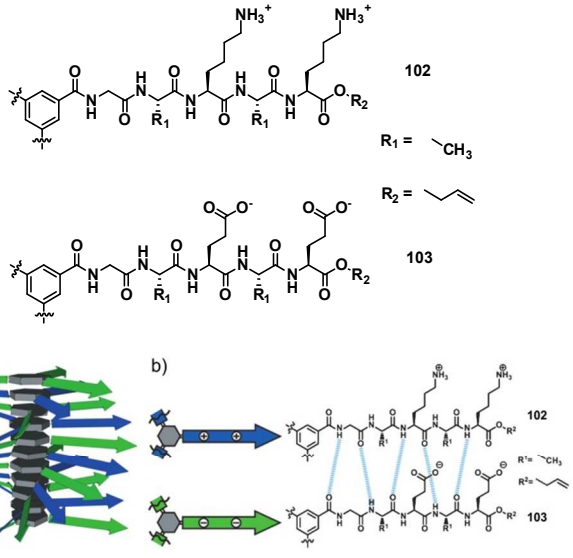

Fig. 32 a) Schematic representation of the supramolecular copolymer and b) the anionic/cationic β-sheet-encoded dendritic co-monomers **102**/**103**. Reproduced with permission from refer. 202 (© Wiley VCH).

The investigation of **102** or **103** in isolation under buffered conditions revealed a CD spectrum that is indicative of a lack of secondary structure. Although the monomeric units are expected to self-assemble by multiple hydrogen bondings between the amide groups, these attractive forces are outbalanced by strong repulsive electrostatic interactions between the anionic side chains in **103** and the cationic substituents in **102**, respectively. As a result, the monomers are unable to self-assemble separately and exist in their monomeric state in buffered solution.
However, if the oppositely charged monomers **102** and **103** are mixed in a 1:1 ratio, an efficient supramolecular copolymerization driven by multiple hydrogen bonding and electrostatic interactions occurs (Fig. 32). As visualized by HRTEM, long one-dimensional nanorods with a uniform diameter of 4 nm are formed. The CD spectrum is characteristic for a hydrogen-bonded parallel β-sheet architecture that is formed in a cooperative fashion. The term "cooperative" was used by the authors to describe the aggregation by multiple non-covalent interactions, although the aggregation mechanism could not be elucidated due to a lack of required statistical theory for the linear copolymerization. On the basis of the overall findings, it seems rational to argue that a cooperative co-

polymerization would most likely occur, since for the co-aggregation attractive electrostatic and directional hydrogen-bonding interactions support each other resulting in one-dimensional structures of high aspect ratio. Theoretical calculations confirmed the contribution of these attractive forces and revealed that water molecules are present between the central aromatic rings precluding further stabilization by π-π-stacking of the aromatic cores.
Interestingly, as a result of the acidic and basic nature of the side chains of the monomers, the copolymers are responsive towards pH changes. Due to their ampholytic character a shift in the pH value of the aqueous media directly results in a change of the ionic character of the molecules and of the self-assembled structures. Monitored by CD studies, the characteristics of parallel β-sheets at neutral pH remain intact in the range of 3.7 to 8.6, however the signal decreases upon leaving neutral conditions due to a weakening of the structures. Finally, at pH 3.6 and 8.9 the copolymers completely disassemble due to the loss of salt bridges between the oppositely-charged subunits, indicated by CD characteristics corresponding to monomeric **102** and **103**. This disassembly was observed to be a reversible process since the co-aggregates can be recovered upon going back to neutral pH range.

Conclusions

In this article, we have reviewed the field of supramolecular polymers by extensively classifying a wide variety of examples depending on the cooperative interactions involved in their self-assembly, with particular emphasis on recent novel strategies introduced in the last half decade. As extracted from these extensive studies, most supramolecular polymers that exhibit a high degree of cooperative are generally based on the following requirement: the repeat monomer units should be capable of establishing various kinds of non-covalent interactions in an orthogonal fashion[203,204] while minimizing possible repulsive interactions. An exception to this rule are purely hydrogen-bonded systems such as the examples reported by Bouteiller and co-workers, whose cooperativity in hydrogen-bonding arises from enthalpic and entropic effects, as described in the introduction.

By far, the most widely used strategy to create supramolecular polymers is the introduction of cooperative π-π- and hydrogen bonding interactions, which has been subject of various review articles[20,38,205] In some cases, if two self-assembled systems that are complementary from the geometric and electronic point of view are mixed, charge-transfer interactions between the donor and acceptor moieties can additionally reinforce the existing π-π- and hydrogen bonding interactions.

Another approach that has been highlighted in this review is the introduction of closed-shell metal ions to self-assembled π-systems. Although numerous examples of self-assembled systems combining metal-metal and π-π-interactions have been reported, it was not until recently when their cooperative aspects were quantitatively examined. Related systems based on metal-ligand and π-π-interactions such as those described by Moore and co-workers also exhibit high levels of cooperativity driven by folding effects of the ligands upon metal coordination.

Interactions involving dipolar or zwitterionic systems in combination with other contributions such as hydrogen bonding, van der Waals or π-π-interactions have been also observed to be a promising strategy towards cooperative supramolecular polymers, as recently reported by the groups of Würthner and Schmuck.

There are a few exceptions of π-systems that self-assemble in a slightly cooperative fashion, although at first glance no secondary interactions are apparently involved. Although the cooperative effects in most of these systems are low, it is believed that conformational changes during the addition of monomers in the stack are the origin of the observed cooperativity.

In the last part, we have dedicated a special section to cooperative supramolecular polymers in aqueous media. Water is a unique media, since in contrast to self-assembled structures in organic solvents, strong hydrophobic interactions themselves can be regarded as an additional driving force to induce cooperative effects. This is clearly demonstrated by some examples in which self- or co-assembled systems based on π-conjugated systems are indeed capable of aggregating in a highly cooperative fashion without the need of introducing additional non-covalent forces other than π-π-interactions.[206]

Very recently, the concept of cooperative self-assembly has been extended to the liquid/solid interface by Yokohama, Hirose and Matsuda,[207] which opens up new possibilities to design highly ordered systems above a critical concentration. We believe that a deep understanding of the non-covalent forces involved in self-assembly processes and their quantitative contribution to cooperative phenomena is a prerequisite to construct increasingly more complex functional supramolecular systems with improved functionalities. Likewise and as recently pointed out by Sugiyasu and Takeuchi, both kinetic and thermodynamic effects should be considered to achieve supramolecular polymers with narrow polydispersity, such as those commonly found in nature.[208]

Acknowledgements

We thank the Humboldt Foundation and the BMBF for financial support and Prof. Frank Würthner for his continuous support and helpful discussions.

Notes and references

Institut für Organische Chemie and Center for Nanosystems Chemistry, Universität Würzburg Am Hubland, 97074 Würzburg (Germany)

1. G. Ercolani, *J. Am. Chem. Soc.*, 2003, **125**, 16097-16103.
2. C. A. Hunter and H. L. Anderson, *Angew. Chem. Int. Ed.*, 2009, **48**, 7488-7499.
3. G. Ercolani and L. Schiaffino, *Angew. Chem. Int. Ed.*, 2011, **50**, 1762-1768.
4. M. F. Perutz, *Q. Rev. Biophys.*, 1989, **22**, 139-236.
5. A. Hernandez-Garcia, D. J. Kraft, A. F. J. Janssen, P. H. H. Bomans, N. A. J. M. Sommerdijk, D. M. E. Thies-Weesie, M. E. Favretto, R. Brock, F. A. de Wolf, M. W. T. Werten, P. van der Schoot, M. C. Stuart and R. de Vries, *Nature Nanotechnol.*, 2014, **9**, 698-702.
6. A. Klug, *Phil. Trans. R. Soc. Lond. B*, 1999, **354**, 531-535.
7. D. E. Sleat, P. C. Turner, J. T. Finch, P. J. Butler and T. M. Wilson, *Virology*, 1986, **155**, 299-308.
8. F. Huber, J. Schnauss, S. Rönicke, P. Rauch, K. Müller, C. Fütterer and J. Käs, *Advances in Physics*, 2013, **62**, 1-112.
9. M. L. Gardel, J.H. Shin, F.C. MacKintosh, L. Mahadevan, P. Matsudaira, and D.A. Weitz, *Science*, 2004, **304**, 1301-1305.
10. T. Aida, E. W. Meijer, S. Stupp, *Science*, 2012, **335**, 813-817.
11. R. M. Macnab, *Annu. Rev. Genet.*, 1992, **26**, 131-158.
12. S. Moens and J. Vanderleyden, *Critical Reviews in Microbiology*, 1996, **22**, 67-100.

13. M. L. DePamphilis and J. Adler, *J. Bacteriol.*, 1971, **105**, 384-395.
14. M. L. DePamphilis and J. Adler, *J. Bacteriol.*, 1971, **105**, 396-407.
15. S. Asakura, G. Eguchi and T. Lino, *J. Mol. Biol.*, 1968, **35**, 227-230.
16. T. Ikeda, S. Asakura and R. Kamiya, *J. Mol. Biol.*, 1985, **184**, 735-737.
17. H. Umeyama and K. Morokuma, J. *Am. Chem. Soc.*, 1977, **99**, 1316-1332.
18. G. R. Desiraju, *Acc. Chem. Res.* 2002, **35**, 565-573.
19. G. R. Desiraju, *Angew. Chem. Int. Ed.,* 2011, **50**, 52-59.
20. T. F. A. de Greef, M. M. J. Smulders, M. Wolffs, A. P. H. J. Schenning, R. P. Sijbesma and E. W. Meijer, *Chem. Rev.*, 2009, **109**, 5687-5754.
21. L. Sarolea-Mathot, *Trans. Faraday Soc*., 1953, **49**, 8.
22. F. Weinhold, J. Mol. Struct. (Theochem), 1997, **398-399**, 181-197.
23. T. Steiner, *Angew Chem Int Ed*, 2002, **41**, 48-76.
24. P. Vishweshwar, A. Nangia and V. M. Lynch Chem. Commun., 2001, 179–180.
25. N.Kobko, L. Paraskevas, E. del Rio and J. J. Dannenberg, *J. Am Chem. Soc*. 2001, **123**, 4348-4349.
26. N.Kobko and J. J. Dannenberg *J. Phys.* Chem. *A*, 2003, **107**, 10389-10395.
27. J. Kříž and J. Dybal, *J. Phys. Chem. B* 2007, **111**, 6118-6126.
28. K. S. Birdi, *Handbook of Surface and Colloid Chemistry - Second Edition* (Chapter 2.6), CRC Press, 2002.
29. G. Gilli, F. Bellucci, V. Ferretti and V. Bertolasi, *J. Am. Chem. Soc.*, 1989, **111**, 1023–1028.
30. V. Bertolasi, P. Gilli, V. Ferretti and G. Gilli, *J. Am. Chem. Soc.*, 1991, **113**, 4917-4925.
31. P. Gilli, V. Bertolasi, V. Ferretti and G. Gilli, *J. Am. Chem. Soc.,* 2000, **122**, 10405-10417.
32. G. Song, L. Zhang, C. He, D.-C. Fang, P. G. Whitten, H. Wang, Macromolecules 2013, **46**, 7423-7435.
33. R. Q. Albuquerque, A. Timme, R. Kress, J. Senker, H.-W. Schmidt, *Chem. Eur. J.*, 2013, **19**, 1647-1657.
34. A. Ciferri, *Macromol. Rapid. Commun*. 2002, **23**, 511-529.
35. D. Zhao and J. S. Moore, *Org. Biomol. Chem.*, 2003, **1**, 3471-3491.
36. Z. Chen, A. Lohr, C. R. Saha-Möller and F. Würthner, *Chem. Soc. Rev.*, 2009, **38**, 564-584.
37. M. M. J. Smulders, M. M. L. Nieuwenhuizen, T. F. A. de Greef, P. van der Schoot, A. P. H. J. Schenning and E. W. Meijer, *Chem. Eur. J.*, 2010, **16**, 362-367.
38. C. Kulkarni, S. Balasubramanian, S. J. George, *ChemPhysChem*, 2013, **14**, 661-673.
39. P. van der Shoot in *Supramolecular Polymers*, A. Ciferri, Ed. (CRC Press, Baton Rouge, LA, 2005).
40. P. Jonkheijm, P. van der Schoot, A. P. H. J. Schenning and E. W. Meijer, *Science*, 2006, **313**, 80-83.
41. M. M. J. Smulders, A. P. H. J. Schenning, and E. W. Meijer, *J. Am. Chem. Soc.*, 2008, **130**, 606-611.
42. H. M. M. ten Eikelder, A. J. Markvoort, T. F. A. de Greef and P. A. J. Hilbers, *J. Phys. Chem. B*, 2012, **116**, 5291-5301.
43. A. J. Markvoort, H. M. M. ten Eikelder, P. A. J. Hilbers, T. F. A. de Greef and E.W. Meijer, *Nat. Commun.*, 2011, **2**, 509-517.
44. R. F. Goldstein and L. Stryer, *Biophys. J.*, 1986, **50**, 583-599.
45. T. E. Kaiser, V. Stepanenko and F. Würthner, *J. Am. Chem. Soc.*, 2009, **131**, 6719-6732.
46. A. P. H. J. Schenning, P. Jonkheijm, E. Peeters and E. W. Meijer, *J. Am. Chem. Soc.*, 2001, **123**, 409-416.
47. P. Jonkheijm, F. J. M. Hoeben, R. Kleppinger, J. Van Herrikhuyzen, A. P. H. J. Schenning and E. W. Meijer, *J. Am. Chem. Soc.*, 2003, **125**, 15491-15949.
48. A. Gesquière, P. Jonkheijm, F. J. M. Hoeben, A. P. H. J. Schenning, S. De Feyter, F. C. Schryer and E. W. Meijer, *Nano Lett.*, 2004, **4**, 1175-1179.
49. F. Oosawa and M. Kasai, *J. Mol. Biol.*, 1962, **4**, 10-21.
50. S. J. George, Ž. Tomović, M. M. J. Smulders, T. F. A. De Greef, P. E. L. G. Leclère, E. W. Meijer and A. P. H. J. Schenning, *Angew. Chem. Int. Ed.*, 2007, **46**, 8206-8211.
51. P. A. Korevaar, S. J. George, A. J. Markvoort, M. M. J. Smulders, P. A. Hilbers, A. P. H. J. Schenning, T. F. A. De Greef and E. W. Meijer, *Nature*, 2012, **481**, 492-496.
52. P. J. M. Stals, J. F. Haveman, R. Martín-Rapún, C. F.C. Fitié, A. R. A. Palmans and E. W. Meijer, *J. Mater. Chem.*, 2009, **19**, 124-130.
53. P. J. M. Stals, M. M. J. Smulders, R. Martín-Rapún, A. R. A. Palmans and E. W. Meijer, *Chem. Eur. J.*, 2009, **15**, 2071-2080.
54. Y. Nakano, T. Hirose, P. J. M. Stals, E. W. Meijer and A. R. A. Palmans, *Chem. Sci*., 2012, **3**, 148-155.
55. T. Mes, M. M. J. Smulders, A. R. A. Palmans and E. W. Meijer, *Macromolecules*, 2010, **43**, 1981-1991.
56. P. J. M. Stals, J. C. Everts, R. de Bruijn, I. A. W. Filot, M. M. J. Smulders, R. Martín-Rapún, E. A. Pidko, T. F. A. De Greff, A. R. A. Palmans, E. W. Meijer, *Chem. Eur. J.*, 2010, **16**, 810-821.
57. D. Ogata, T. Shikata and K. Hanabusa, *J. Phys. Chem. B*, 2004, **108**, 15503-15510.
58. Y. Matsunaga, N. Miyajima, Y. Nakayasu, S. Sakai, M. Yonenaga, *Bull. Chem. Soc. Jpn.* 1988, **61**, 207-210.
59. A. J. Wilson, M. Masuda, R. P. Sijbesma and E. W. Meijer, *Angew. Chem. Int. Ed.*, 2005, **44**, 2275-2279.
60. M. M. J. Smulders, I. A. W. Filot, J. M. A. Leenders, P. van der Schoot, A. R. A. Palmans, A. P. H. J. Schenning and E. W. Meijer *J. Am. Chem. Soc.*, 2010, **132**, 611-619.
61. M. M. J. Smulders, M. M. L. Nieuwenhuizen, M. Grossman, I. A. W. Filot, C. C. Lee, T. F. De Greef, A. P. H. J. Schenning, A. R. A. Palmans and E. W. Meijer, *Macromolecules*, 2011, **44**, 6581-6587.
62. T. Mes, S. Cantekin, D. W. R. Balkenende, M. M. M. Frissen, M. A. J. Gillissen, B. F. M. De Waal, I. K. Voets, E. W. Meijer and A. R. A. Palmans, *Chem. Eur. J.*, 2013, **19**, 8642-8649.
63. H.-J. Lee, Y.-S. Choi, K.-B. Lee, J. Park, C.-J. Yoon, *J. Phys. Chem. A*, 2002, **106**, 7010-7017.
64. S. Boileau, L. Bouteiller, F. Lauprêtre and F. Lortie, *New. J. Chem.*, 2000, **24**, 845-848.
65. F. Lortie, S. Boileau, L. Bouteiller, C. Chassenieux, B. Demé, G. Ducouret, M. Jalabert, F. Lauprêtre and P. Terech, *Langmuir*, 2002, **18**, 7218-7222.
66. V. Simic, L. Bouteiller and M. Jalabert, *J. Am. Chem. Soc.*, 2003, **125**, 13148-13154.
67. O. Colombani and L. Bouteiller, *New. J. Chem.*, 2004, **28**, 1373-1382.
68. L. Bouteiller, O. Colombani, F. Lortie and P. Terech, *J. Am. Chem. Soc.*, 2005, **127**, 8893-8898.
69. P. van der Schoot, M. A. J. Michels, L. Brunsveld, R. P. Sijbesma, and A. Ramzi, *Langmuir* 2000, **16**, 10076-10083.

70. J. van Gestel, P. van der Schoot and M. A. J. Michels, *J. Phys. Chem. B*, 2001, **105**, 10691-10699.
71. B. Isare, M. Linares, L. Zargarian, S. Fermandjian, M. Miura, S. Motohashi, N. Vanthuyne, R. Lazzaroni and L. Bouteiller, *Chem. Eur. J.*, 2010, **16**, 173-177.
72. M. Roman, C. Cannizzo, T. Pinault, B. Isare, B. Andrioletti, P. van der Schoot and L. Bouteiller, *J. Am. Chem. Soc.*, 2010, **132**, 16818-16824.
73. F. Würthner, *Chem. Commun.*, 2004, 1564-1579.
74. F. Würthner, T. E. Kaiser and C. R. Saha-Möller, *Angew. Chem. Int. Ed.*, 2011, **50**, 3376-3410.
75. D. Görl, X. Zhang and F. Würthner, *Angew. Chem. Int. Ed.*, 2012, **51**, 6328-6348.
76. Z. Chen, B. Fimmel, F. Würthner, Org. Biomol. Chem., 2012, 10, 5845-5855.
77. T. E. Kaiser, H. Wang, V. Stepanenko and F. Würthner, *Angew. Chem. Int. Ed.*, 2007, **46**, 5541-5544.
78. F. Fennel, S. Wolter, Z. Xie, P.-A. Plötz, O. Kühn, F. Würthner and S. Lochbrunner, *J. Am. Chem. Soc.*, 2013, **135**, 18722-18725.
79. T. Seki, A. Asano, S. Seki, Y. Kikkawa, H. Murayama, A. Kitamura and S. Yagai, *Chem. Eur. J.*, 2011, **17**, 3598-3608.
80. C. Shao, M. Stolte and F. Würthner, *Angew. Chem. Int. Ed.*, 2013, **52**, 10463-10467.
81. R. van der Weegen, P. A. Korevaar, P. Voudouris, I. K. Voets, T. F. A. de Greef, J. A. J. M. Vekemans and E. W. Meijer, *Chem. Commun.*, 2013, **49**, 5532-5534.
82. F. Würthner, C. Thalacker, S. Diele and C. Tschierske, *Chem. Eur. J.*, 2001, **7**, 2245-2253.
83. Z. Chen, V. Stepanenko, V. Dehm, P. Prins, L. D. A. Siebbeles, J. Seibt, P. Marquetand, V. Engel and F. Würthner, *Chem. Eur. J.*, 2007, **13**, 436-449.
84. S. Yagai, M. Suzuki, X. Lin, M. Gushiken, T. Noguchi, T. Karatsu, A. Kitamura, A. Saeki, S. Seki, Y. Kikkawa, Y. Tani and K.-i. Nakayama, *Chem. Eur. J.*, 2014, **20**, 16128-16137.
85. M. Yamauchi, S. Kubota, T. Karatsu, A. Kitamura, A. Ajayaghosh and S. Yagai, *Chem. Commun.*, 2013, **49**, 4941-4943.
86. T. Seki, X. Lin and S. Yagai, *Asian. J. Org. Chem.*, 2013, **2**, 708-724.
87. S. Yagai, M. Gushiken, T. Karatsu, A. Kitamura and Y. Kikkawa, *Chem. Commun.*, 2011, **47**, 454-456.
88. S. Yagai, M. Usui, T. Seki, H. Murayama, Y. Kikkawa, S. Uemura, T. Karatsu, A. Kitamura, A. Asano and S. Seki, *J. Am. Chem. Soc.*, 2012, **134**, 7983-7994.
89. G. Fernández, F. García, F. Aparicia, E. Matesanz and L. Sánchez, *Chem. Commun.*, 2009, 7155-7157.
90. F. García, G. Fernández and L. Sánchez, *Chem. Eur. J.*, 2009, **15**, 6740-6747.
91. F. García and L. Sánchez, *Chem. Eur. J.*, 2010, **16**, 3138-3146.
92. F. García, J. Buendía and L. Sánchez, *J. Org. Chem.*, 2011, **76**, 6271-6276.
93. J. Buendía and L. Sánchez, *Org. Lett.*, 2013, **15**, 5746-5749.
94. F. Aparicio, F. García and L. Sánchez, *Chem. Eur. J.*, 2013, **19**, 3239-3248.
95. F. García, P. M. Viruela, E. Matesanz, E. Ortí and L. Sánchez, *Chem. Eur. J.*, 2011, **17**, 7755-7759.
96. M. M. J. Smulders, P. J. M. Stals, T. Mes, T. F. E. Paffen, A. P. H. J. Schenning, A. R. A. Palmans and E. W. Meijer, *J. Am. Chem. Soc.*, 2010, **132**, 620-626.
97. F. García and L. Sánchez, *J. Am. Chem. Soc.*, 2012, **134**, 734-742.
98. F. García, P. A. Korevaar, A. Verlee, E. W. Meijer, A. R. A. Palmans and L. Sánchez, *Chem. Commun.*, 2013, **49**, 8674-8676.
99. F. Wang, M. A. J. Gillissen, P. J. M. Stals, A. R. A. Palmans and E. W. Meijer, *Chem. Eur. J.*, 2012, **18**, 11761-11770.
100. F. Aparicio, E. Matesanz and L. Sánchez, *Chem. Commun.*, 2012, **48**, 5757-5759.
101. F. Aparicio and L. Sánchez, *Chem. Eur. J.*, 2013, **19**, 10482-10486.
102. M. R. Molla, A. Das and S. Ghosh, *Chem. Eur. J.*, 2010, **16**, 10084-10093.
103. M. R. Molla and S. Ghosh, *Chem. Eur. J.*, 2012, **18**, 9860-9869.
104. A. Das, M. R. Molla, A. Banerjee, A. Paul and S. Ghosh, *Chem. Eur. J.*, 2011, 17, 6061-6066.
105. H. Kar and S. Ghosh, *Chem. Commun.*, 2014, **50**, 1064-1066.
106. A. Das and S. Ghosh, *Angew. Chem. Int. Ed.*, 2014, **53**, 1092-1097.
107. P. Rajdev, M. R. Molla and S. Ghosh, *Langmuir*, 2014, **30**,1969-1976.
108. A. Das, M. R. Molla, B. Maity, D. Koley and S. Ghosh, *Chem. Eur. J.*, 2012, **18**, 9849-9859.
109. K. Jalani, M. Kumar and S. J. George, *Chem. Commun.*, 2013, **49**, 5174-5176.
110. M. Kumar, K. V. Rao and S. J. George, *Phys. Chem. Chem. Phys.*, 2014, **16**, 1300-1313.
111. A. Das and S. Ghosh, *Angew. Chem. Int. Ed.*, 2014, **53**, 2038-2054.
112. S. S. Babu, V. K. Praveen and A. Ajayaghosh, *Chem. Rev.*, 2014, **114**, 1973-2129.
113. S. S. Babu, S. Prasanthkumar and A. Ajayaghosh, *Angew. Int. Chem. Ed.*, 2012, **51**, 1766-1776.
114. V. K. Praveen and A. Ajayaghosh, *Acc. Chem. Res.*, 2007, **40**, 644–656.
115. F. García, J. Buendía, S. Ghosh, A. Ajayaghosh and L. Sánchez, *Chem. Commun.*, 2013, **49**, 9278-9280.
116. J. Puigmartí-Luis, E. E. Laukhina, V. N. Laukhin, Á. P. del Pino, N. Mestres, J. Vidal-Gancedo, C. Rovira and D. B. Amabilino, *Adv. Funct. Mater.*, 2009, **19**, 934-941.
117. J. Puigmartí-Luis, Á. P. del Pino, E. Laukhina, J. Esquena, V. Laukhin, C. Rovira, J. Vidal-Gancedo, A. G. Kanaras, R. J. Nichols, M. Brust and D. B. Amabilino, *Angew. Chem. Int. Ed.*, 2008, **47**, 1861-1865.
118. J. Puigmartí-Luis, V. Laukhin, Á. P. del Pino, J. Vidal-Gancedo, C. Rovira, E. Laukhina and D. B. Amabilino, *Angew. Chem. Int. Ed.*, 2007, **46**, 238-241.
119. I. Danila, F. Riobé, F. Piron, J. Puigmartí-Luis, J. D. Wallis, M. Linares, H. Ågren, D. Beljonne, D. B. Amabilino and N. Avarvari, *J. Am. Chem. Soc.*, 2011, **133**, 8344-8353.
120. R. Chakrabarty, P. S. Mukherjee and P. J. Stang, *Chem. Rev.*, 2011, **111**, 6810-6918.
121. M. J. Mayoral, G. Fernández, *Chem. Sci.*, 2012, **3**, 1395-1398.
122. M. Amelia, L. Zou and A. Credi, *Coor. Chem. Rev.*, 2010, **254**, 2267-2280.
123. M. Higuchi, *J. Mater. Chem. C*, 2014, **2**, 9331-9341.
124. B. Happ, A. Winter, M. D. Hager and U. S. Schubert, *Chem. Soc. Rev.*, 2012, **41**, 2222-2255.

125. J. K.-H. Hui and M. J. MacLachlan, *Coor. Chem. Rev.*, 2010, **254**, 2363-2390.
126. I. Eryazici, C. N. Moorefield and G. R. Newkome, *Chem. Rev.*, 2008, **108**, 1834-1895.
127. M. Mauro, A. Aliprandi, D. Septiadi, N. S. Kehr and L. De Cola, *Chem. Soc. Rev.*, 2014, **43**, 4144-4166.
128. A. Y.-Y. Tam and V. W.-W. Yam, *Chem. Soc. Rev.*, 2013, **42**, 1540-1567.
129. K. M.-C. Wong and V. W.-W. Yam, *Acc. Chem. Res.*, 2011, **44**, 424-434.
130. C. M. Che and S. W. Lai, *Coord. Chem. Rev.*, 2005, **249**, 1296-1309.
131. A. Kishimura, T. Yamashita and T. Aida, *J. Am. Chem. Soc.*, 2005, **127**, 179-183.
132. A. Kishimura, T. Yamashita, K. Yamaguchi and T. Aida, *Nature*, 2005, **4**, 546-549.
133. Y. Li, D. P.-K. Tsang, C. K.-M. Chan, K. M.-C. Wong, M.-Y. Chan and V. W.-W. Yam, *Chem. Eur. J.*, 2014, **42**, 13710-13715.
134. C. Y.-S. Chung and V. W.-W. Yam, *Chem. Eur. J.*, 2014, **20**, 13016-13027.
135. S. Y.-L. Leung, A. Y.-Y. Tam, C.-H. Tao, H. S. Chow and V. W.-W. Yam, *J. Am. Chem. Soc.*, 2012, **134**, 1047-1056.
136. C. A. Strassert, C.-H. Chien, M. D. G. Lopez, D. Kourkoulos, D. Hertel, K. Meerholz and L. De Cola, *Angew. Chem. Int. Ed.*, 2011, **50**, 946-950.
137. N. K. Allampally, M. Bredol, C. A. Strassert and L. De Cola, *Chem. Eur. J.*, 2014, **20**, 16863-16868.
138. I. Stengel, C. A. Strassert, L. De Cola and P. Bäuerle, *Organometallics*, 2014, **33**, 1345-1355.
139. X.-S. Xiao, W. Lu and C.-M. Che, *Chem. Sci.*, 2014, **5**, 2482-2488.
140. G. Cheng, S. C. F. Kui, W.-H. Ang, M.-Y. Ko, P.-K. Chow, C.-L. Kwong, C.-C. Kwok, C. Ma, X. Guan, K.-H. Low, S.-J. Su and C.-M. Che, *Chem. Sci.*, 2014, **5**, 4819-4830.
141. Y. Chen, W. Lu and C.-M. Che, *Organometallics*, 2013, **32**, 350-353.
142. N. K. Allampally, C.-G. Daniliuc, C. A. Strassert, *doi:10.1021/ic 5025636.*
143. M. J. Mayoral, C. Rest, V. Stepanenko, J. Schellheimer, R. Q. Albuquerque and G. Fernández, *J. Am. Chem. Soc.*, 2013, **135**, 2148-2151.
144. Y.-J. Tian, E. W. Meijer and F. Wang, *Chem. Commun.*, 2013, **49**, 9197-9199.
145. X.-D. Xu, J. Zhang, L.-J. Chen, X.-L. Zhao, D.-X. Wang and H.-B. Yang, *Chem. Eur. J.*, 2012, **18**, 1659-1667.
146. M. T. Stone and J. S. Moore, *J. Am. Chem. Soc.*, 2005, **127**, 5928-5935.
147. J. W. Wackerly and J. S. Moore, *Macromolecules*, 2006, **39**, 7269-7276.
148. J. C. Nelson, J. G. Saven, J. S. Moore and P. G. Wolynes, *Science*, 1997, **227**, 1793-1796.
149. D. Poland, H. A. Scheraga, *Theory of Helix-Coil Transitions in Biopolymers*; Academic Press: New York, 1970.
150. R. B. Prince, J. G. Saven, P. G. Wolynes and J. S. Moore, *J. Am. Chem. Soc.*, 1999, **121**, 3114-3121.
151. K. Matsuda, M. T. Stone and J. S. Moore, *J. Am. Chem. Soc.*, 2002, **124**, 11836-11837.
152. C. G. Spike and R. W. Parry, *J. Am. Chem. Soc.*, 1953, **75**, 3770-3772.
153. A. W. Adamson, *J. Am. Chem. Soc.*, 1954, **76**, 1578-1579.
154. A. Lohr, M. Lysetska and F. Würthner, *Angew. Chem. Int. Ed.*, 2005, **44**, 5071-5074.
155. A. Lohr and F. Würthner, *Chem. Commun.*, 2008, 2227-2229.
156. J. Seibt, A. Lohr, F. Würthner and V. Engel, *Phys. Chem. Chem. Phys.*, 2007, **9**, 6214-6218.
157. A. Lohr, T. Gress, M. Deppisch, M. Knoll and F. Würthner, *Synthesis*, 2007, **19**, 3073-3082.
158. A. Lohr and F. Würthner, *Angew. Chem. Int. Ed.*, 2008, **47**, 1232-1236.
159. A. Lohr, S. Uemura and F. Würthner, *Angew. Chem. Int. Ed.*, 2009, **48**, 6165-6168.
160. A. Lohr and F. Würthner, *Isr. J. Chem.*, 2011, **51**, 1052-1066.
161. A. Lohr, M. Grüne and F. Würthner, *Chem. Eur. J.*, 2009, **15**, 3691-3705.
162. F. Würthner, S. Yao and U. Beginn, *Angew. Chem. Int. Ed.*, 2003, **42**, 3247-3250.
163. G. Fernández, M. Stolte, V. Stepanenko and F. Würthner, *Chem. Eur. J.*, 2013, **19**, 206-217.
164. R. Schmidt, S. Uemura and F. Würthner, *Chem. Eur. J.*, 2010, **16**, 13706-13715.
165. C. Schmuck, *Eur. J. Org. Chem.*, 1999, 2397-2403.
166. C. Schmuck, *J. Org. Chem.*, 2000, **65**, 2432-2437.
167. C. Schmuck, *Tetrahedron*, 2001, **57**, 3063-3067.
168. C. Schmuck and W. Wienand, *J. Am. Chem. Soc.*, 2003, **125**, 452-459.
169. S. Schlund, C. Schmuck and B. Engels, *J. Am. Chem. Soc.*, 2005, **127**, 11115-11124.
170. C. Schmuck, T. Rehm, F. Gröhn, K. Klein and F. Reinhold, *J. Am. Soc. Chem.*, 2006, **128**, 1430-1431.
171. C. Schmuck, *Coor. Chem. Rev.*, 2006, **250**, 3053-3067.
172. T. H. Rehm and C. Schmuck, *Chem. Soc. Rev.*, 2010, **39**, 3597-3611.
173. M. T. Fenske, W. M.-Zaika, H.-G. Korth, H. Vieker, A. Turchanin and C. Schmuck, *J. Am. Chem. Soc.*, 2013, **135**, 8342-8349.
174. P. J. M. Stals, P. A. Korevaar, M. A. J. Gillissen, T. F. A. De Greef, C. F. C. Fitié, R. P. Sijbesma, A. R. A. Palmans and E. W. Meijer, *Angew. Chem. Int. Ed.*, 2012, **51**, 11297-11301.
175. F. Aparicio, F. García, G. Fernández, E. Matesanz and L. Sánchez, *Chem. Eur. J.*, 2011, **17**, 2769-2776.
176. G. Fernández, F. García, L. Sánchez, *Chem. Commun.*, 2008, 468-470.
177. F. Garcia, F. Aparicio, G. Fernández and L. Sánchez, *Org. Lett.*, 2009, **11**, 2748-2751.
178. C. Shao, M. Stolte and F. Würthner, *Angew. Chem. Int. Ed.*, 2013, **52**, 7482-7486.
179. Ž. Tomović, J. van Dongen, S. J. George, H. Xu, W. Pisula, P. Leclère, M. M. J. Smulders, S. De Feyter, E. W. Meijer, and A. P. H. J. Schenning, *J. Am. Chem. Soc.*, 2007, **129**, 16190-16196.
180. Lazaridis, in *eLS*, John Wiley & Sons, 2013.
181. K. A. Dill, *Biochemistry*, 1990, **29**, 7133-7155.
182. D. Chandler, *Nature*, 2005, **437**, 640-647.
183. P. Ball, *Chem. Rev.*, 2008, **108**, 74-108.
184. R. Ludwig, *Angew. Chem.*, 2001, 113, 1856-1876; *Angew. Chem. Int. Ed.*, 2001, 40, 1808-1827.

185. J.-H. Ryu, D.-J. Hong and M. Lee, *Chem. Commun.*, 2008, 1043-1054.
186. H. J. Kim, T. Kim and M. Lee, *Acc. Chem. Res.*, 2011, **44**, 72-82.
187. W. Li, Y. Kim, J. Li and M. Lee, *Soft Matter*, 2014, **10**, 5231-5242.
188. G. V. Oshovsky, D. N. Reinhoudt and W. Verboom, *Angew. Chem. Int. Ed.*, 2007, **46**, 2366-2393.
189. T. Rehm and C. Schmuck, *Chem. Commun.*, 2008, 801-813.
190. E. Krieg and B. Rybtchinski, *Chem. Eur. J.*, 2011, **17**, 9016-9026.
191. C. Rest, M. J. Mayoral and G. Fernández, *Int. J. Mol. Sci.*, 2013, **14**, 1541-1565.
192. J. B. Matson and S. I. Stupp, *Chem. Commun.*, 2012, **48**, 26-33.
193. X. Ma and H. Tian, *Acc. Chem. Res.*, 2014, **47**, 1971-1981.
194. X. Zhang, D. Görl and F. Würthner, *Angew. Chem.*, 2014, **126**, 1294-1298; *Angew. Chem. Int. Ed.*, 2014, **53**, 1270–1274.
195. M. J. Mayoral, C. Rest, J. Schellheimer, V. Stepanenko and G. Fernández, *Chem. Eur. J.*, 2012, **18**, 15607-15611.
196. N. K. Allampally, A. Florian, M. J. Mayoral, C. Rest, V. Stepanenko, G. Fernández, *Chem. Eur. J.*, 2014, **20**, 10669-10678.
197. E. Krieg, H. Weissman, E. Shimoni, A. B. O. Ustinov and B. Rybtchinski, *J. Am. Chem. Soc.*, 2014, **136**, 9443-9452.
198. C. Rest, M. J. Mayoral, K. Fucke, J. Schellheimer, V. Stepanenko and G. Fernández, *Angew. Chem. Int. Ed.*, 2014, **53**, 700-705; *Angew. Chem.*, 2014, **126**, 716-722.
199. C. Rest, A. Martin, V. Stepanenko, N. K. Allampally, D. Schmidt and G. Fernández, *Chem. Commun.*, 2014, **50**, 13366-13369.
200. P. Besenius, G. Portale, P. H. H. Bomans, H. M. Janssen, A. R. A. Palmans and E. W. Meijer, *Proc. Nat. Acad. Sci.*, 2010, **107**, 17888-17893.
201. P. Besenius, K. P. van den Hout, H. M. H. G., Albers, T. F. A. De Greef, L. L. C. Olijve, T. M. Hermans, B. F. M. de Waal, P. H. H. Bomans, N. A. J. M. Sommerdijk, G. Portale, A. R. A. Palmans, M. H. P. van Genderen, J. A. J. M. Vekemans and E. W. Meijer, *Chem. Eur. J.*, 2011, **17**, 5193-5203.
202. H. Frisch, J. P. Unsleber, D. Lüdeker, M. Peterlechner, G. Brunklaus, M. Waller and P. Besenius, *Angew. Chem. Int. Ed.*, 2013, **52**, 10097-10101.
203. E. Elacqua, D. S. Lye and Marcus Weck, *Acc. Chem. Res.*, 2014, **47**, 2405–2416.
204. S-L. Li, T. Xiao, C. Lin and L. Wang, *Chem. Soc. Rev.*, 2012, **41**, 5950–5968.
205. D. Gonzalez-Rodriguez and A. P. H. J. Schenning, *Chem. Mater.*, 2011, **23**, 310–325.
206. T. Rudolph, N. K. Allampally, G. Fernández and F. H. Schacher, *Chem. Eur. J.*, 2014, **20**, 13871-13875.
207. S. Yokohama, T. Hirose and K. Matsuda, *Chem. Commun.*, 2014, **50**, 5964-5966.
208. S. Ogi, K. Sugiyasu, S. Manna, S. Samitsu and M. Takeuchi, *Nature Chem.*, 2014, **8**, 188-195.

